

1 **Stormflow response and ‘effective’ hydraulic conductivity of a degraded tropical**
2 ***Imperata* grassland catchment as evaluated with two infiltration models**

3

4 Zhuo Cheng^{1,2}, Jun Zhang^{3,4,*}, Bofu Yu², Nick A. Chappell⁵,
5 H.J. (Ilja) van Meerveld⁶, and L. Adrian Bruijnzeel^{3,7}

6

7 ¹*Department of Geography, Beijing Normal University, Beijing, P. R. China*

8 ²*Australian Rivers Institute and School of Engineering and Built Environment,*
9 *Griffith University, Brisbane, Australia*

10 ³*Institute of International Rivers and Eco-Security, Yunnan University, Kunming, P.*
11 *R. China*

12 ⁴*Environmental Modelling, Sensing & Analysis, TNO, Petten, The Netherlands*

13 ⁵*Lancaster Environment Centre, University of Lancaster, Lancaster, United Kingdom*

14 ⁶*Department of Geography, Hydrology and Climate, University of Zurich, Zurich,*
15 *Switzerland*

16 ⁷*Department of Geography, King’s College London, London, United Kingdom*

17

18 Corresponding author: Jun Zhang (jzg290@outlook.com)

19

20 **Key points:**

- 21 • The Spatially Variable Infiltration model outperformed the Green–Ampt
22 model when simulating hydrographs, especially for multi-peak events.
23 • SVI-model parameter values varied markedly, but were correlated with
24 antecedent topsoil moisture content
25 • Model-derived infiltration capacities were much higher than field-measured
26 K_{sat} , regardless of the model or field method used

27 **Abstract**

28 Predicting catchment stormflow responses after tropical deforestation remains
29 difficult. We used five-minute rainfall and storm runoff data for 30 events to calibrate
30 the Green–Ampt (GA) and the Spatially Variable Infiltration (SVI) model and predict
31 runoff responses for a small, degraded grassland catchment on Leyte Island (the
32 Philippines), where infiltration-excess overland flow is considered the dominant storm
33 runoff generating process. SVI replicated individual stormflow hydrographs better
34 than GA, particularly for events with a small runoff response or multiple peaks.
35 Calibrated parameter values of the SVI model (*i.e.*, spatially averaged maximum
36 infiltration capacity, I_m and initial abstraction, F_0) varied markedly between events,
37 but exhibited significant negative linear correlations with (mid-slope) soil water
38 content at 10 cm (SWC_{10}) – as did the ‘catchment effective’ hydraulic conductivity
39 (K_e) of the GA model. SWC_{10} -based values of F_0 and I_m in SVI resulted in
40 satisfactory to good predictions ($NSE > 0.50$) for 18 out of 26 storms for which data
41 on SWC_{10} were available, but failed to reproduce the hydrographs for six events
42 (23%) with mostly small runoff responses. Median values of field-measured near-
43 surface K_{sat} ($\sim 2\text{--}3\text{ mm h}^{-1}$, depending on method) were distinctly lower than the
44 median I_m (32 mm h^{-1}) and, to a lesser extent, K_e ($\sim 8\text{ mm h}^{-1}$), confirming previously
45 suspected under-estimation of field-measured K_{sat} . Using pre-storm topsoil moisture
46 content and 5-min rainfall intensities as the driving variables to model infiltration with
47 SVI gave more realistic results than the classic GA approach or the comparison of
48 rainfall intensities with field-measured K_{sat} .

49

50 **Plain Language Summary**

51 It is important for flood management to be able to predict the volume and peak value
52 of streamflow during intense rainfall (so-called ‘stormflow’). We used rainfall and
53 streamflow data for a small, degraded tropical grassland catchment on Leyte Island
54 (the Philippines) to calibrate two rainfall infiltration models of different complexity:
55 the simple Green–Ampt model (GA) and the Spatially Variable Infiltration (SVI)
56 model that describes rainfall infiltration into the soil as a function of the intensity of
57 the rain. SVI generally performed better than GA in simulating observed stormflow
58 responses, especially for events with multiple rainfall peaks. Values for the two main
59 parameters of SVI (the amount of rainfall required to initiate stormflow, and the
60 maximum infiltration capacity of the soil) varied with the amount of moisture in the
61 top 10 cm of the soil prior to the rain. Using the measured topsoil moisture contents
62 for 26 rainfall events to estimate the SVI parameter values and predict the stormflow
63 response from the measured rainfall intensity produced satisfactory to good results for
64 ~70% of the examined storms. However, it failed to reproduce the stormflow patterns
65 for six events with mostly small to very small runoff responses.

66

67 **1 Introduction**

68 Large areas in the humid and seasonal tropics suffer moderate to severe soil
69 degradation (Bai et al., 2008; Gibbs & Salmon, 2015). Repeated cycles of slash-and-
70 burn cultivation, as well as more intensive forms of agricultural cropping and grazing,
71 have resulted in reductions in topsoil organic matter content, soil faunal activity and
72 macroporosity, and an increase in bulk density (Martinez & Zinck, 2004;
73 Shougrakpam et al., 2010; Recha et al., 2012; Zwartendijk et al., 2017; Toohey et al.,
74 2018). The associated decline in soil infiltration capacity typically leads to increased
75 occurrence and amounts of infiltration-excess overland flow (IOF) in regions and/or
76 periods with high rainfall intensities (Chandler & Walter, 1998; Ziegler et al., 2004;
77 Molina et al., 2007; Ghimire et al., 2013; Bush et al., 2020). IOF, in turn, causes
78 accelerated erosion, as well as higher runoff peaks at the headwater catchment scale
79 (Ziegler et al., 2009; Liu et al., 2011; Recha et al., 2012; Ribolzi et al., 2017; Birch et
80 al., 2021a, 2021b), which exacerbates flooding and sedimentation problems
81 downstream (Bruijnzeel, 2004; Sidle et al., 2006; Valentin et al., 2008; Yin et al.,
82 2019).

83 Despite the extent of tropical land degradation and associated environmental
84 problems, comparatively little progress has been made with the quantitative prediction
85 of storm runoff for degraded tropical catchments (Yu, 2005; Sidle et al., 2006; Ribolzi
86 et al., 2017; Yamamoto et al., 2021; Birch et al., 2021a). Some of the more frequently
87 used approaches include the Green–Ampt infiltration model (GA; Mein & Larsen,
88 1973; Chu, 1978) and the US Soil Conservation Service curve number (SCS–CN)
89 method (Ponce & Hawkins, 1996). GA partitions rainfall between infiltration and
90 IOF. The SCS–CN method estimates ‘direct runoff’ (*i.e.*, a fast runoff component that
91 is assumed to be linearly related to rainfall) from hillside plots or small catchments
92 using a dimensionless ‘curve number’ (CN-value) that is assumed to capture
93 catchment-wide water retention as a function of soil texture, drainage conditions and
94 land cover/use (Ponce & Hawkins, 1996). Both approaches have their limitations.
95 Although GA takes short-term changes in infiltration rate as the soil wets up during

96 rainfall into account (Koorevaar et al., 1983), the method applies only to individual
97 points. The notoriously high spatial variability of near-surface saturated soil hydraulic
98 conductivity (K_{sat}) makes it difficult to obtain ‘representative’ estimates at the
99 hillslope- to catchment scale (Sharma et al., 1987; Dunne et al., 1991; Chappell et al.,
100 1998; Zehe & Flühler, 2001; Campos Pinto et al., 2018). Hence, a spatially uniform
101 ‘effective’ final infiltration rate (K_c) is usually assumed in catchment-scale
102 applications of GA (Aston & Dunin, 1979; James et al., 1992; Nearing et al., 1996;
103 Leemhuis et al., 2007; Yira et al., 2016). More importantly, once infiltration reaches
104 steady-state condition, infiltration rates as predicted by GA do not respond to changes
105 in rainfall input anymore (Yu, 1999), despite ample evidence to the contrary
106 (Hawkins, 1982; Dubrueil, 1985; Dunne et al., 1991; Yu et al., 1997a; Stone et al.,
107 2008). On the other hand, the SCS–CN method is incapable of providing information
108 on the spatio-temporal variation in storm runoff (Garen & Moore, 2005; Ogden et al.,
109 2017). Nevertheless, GA or SCS–CN constitute a core element of widely used erosion
110 and hydrological models, such as WEPP (Flanagan et al., 2001; Nearing et al., 1996)
111 and SWAT (Neitsch et al., 2011; Arnold et al., 2012). Therefore, Ogden et al. (2017)
112 called for the identification of ‘*more appropriate dynamic hydrological formulations*
113 *for different hydro-geographic regions*’ (such as the tropics) to replace the static and
114 spatially lumped SCS–CN method, as did Yu (1999) in relation to GA (*cf.* Yamamoto
115 et al., 2020).

116 Arguably, in areas with significant surface degradation, where IOF is likely to be the
117 dominant storm runoff generation mechanism (Sutherland & Bryan, 1990; Mathys et
118 al., 1996; Chandler & Walter, 1998; Molina et al., 2007), a dynamic model of
119 infiltration that takes the spatial variability of surface K_{sat} into account, *as well as* the
120 positive impact of rainfall intensity on infiltration rates (Hawkins, 1982; Dunne et al.,
121 1991), would go some way towards the improved process description called for by
122 Ogden et al. (2017). Building upon earlier work by Hawkins and Cundy (1987), Yu et
123 al. (1997a) developed a spatially variable infiltration model (SVI) that relates actual
124 infiltration rates at the plot scale (as determined by subtracting measured IOF from

125 rainfall over short consecutive periods) to rainfall intensity and a spatially averaged
126 infiltration parameter. SVI proved to be consistently superior to GA with regard to
127 predicting IOF from (mostly large) storms on (mostly bare) hillside plots at various
128 tropical sites (Yu, 1999). Fentie et al. (2002) considered SVI the best choice amongst
129 eight different methods to predict IOF from grazed plots in Queensland, whereas Van
130 Dijk and Bruijnzeel (2004) concluded that SVI provided a ‘*robust and accurate*
131 *method for predicting runoff*’ from terraced fields on volcanic substrate in Indonesia.
132 Recently, Z. Cheng et al. (2018) compared the performance of GA and SVI under
133 much drier conditions on the Chinese Loess Plateau, and concluded that the amount of
134 simulated IOF was less sensitive to changes in model parameter values for SVI than
135 for GA. Despite SVI’s superior performance at the plot scale in a range of tropical
136 settings (Yu, 1999; Fentie et al., 2002; Van Dijk & Bruijnzeel, 2004; cf. Patin et al.,
137 2012), the model has so far not been used to predict stormflow at the *catchment scale*.
138 Conversely, GA has been used extensively for this purpose (*e.g.*, Aston & Dunin,
139 1979; Van Mullem, 1991; James et al., 1992; Obiero, 1996; Conolly et al., 1997;
140 Leemhuis et al., 2007; Yira et al., 2016; Yamamoto et al., 2020).

141
142 This paper marks the first attempt to evaluate SVI’s ability to predict stormflow
143 hydrographs and peak discharge, using detailed rainfall and streamflow data for the
144 3.2 ha Basper catchment on Leyte Island (the Philippines). After decades of slash-
145 and-burn, much of the catchment is covered by *Imperata* and *Saccharum* grasses.
146 Fire-climax grasslands constitute a widespread form of degraded land, occupying an
147 estimated area of up to 57 million ha across South and Southeast Asia in the early
148 1990s (Garrity et al., 1997). More than two-thirds of the estimated 6.5 million ha
149 under *Imperata* in the Philippines (17% of the national land base) were classified as
150 experiencing moderate to severe surface erosion (Concepcion & Samar, 1995).
151 Despite its widespread existence, quantitative hydrological information for this type
152 of grassland is scant (Jasmin, 1976; Lim Suan, 1995; cf. Sirimarco et al., 2018).
153 Earlier work in the Basper catchment revealed very low (near-) surface values of K_{sat} ,
154 suggesting the likelihood of frequent IOF occurrence, even though K_{sat} may have been
155 under-estimated (Zhang et al., 2019a). Nearly two-thirds of the annual streamflow at

156 Basper consists of stormflow (here defined as the component of the hydrograph above
157 the Hewlett and Hibbert (1967) separation line), rendering the catchment one of the
158 hydrologically most responsive humid tropical sites described to date (Zhang et al.,
159 2018a; *cf.* Chappell et al., 2012; Birkel et al., 2021). Although no explicit
160 measurements of hillslope IOF were made at Basper, the extreme dilution of
161 streamflow during rainfall events (Zhang et al., 2018a; Van Meerveld et al., 2019) and
162 isotope hydrography separation results (Van Meerveld et al., 2019) all suggest a major
163 contribution of low electrical conductivity ‘new water’ to stormflow. Hence, our
164 objectives were to: (i) test the appropriateness and relative performance of GA and
165 SVI for describing storm runoff for a small catchment in a state of advanced surface
166 degradation; (ii) examine the temporal variability of the calibrated model parameters,
167 and their relationships with antecedent soil water content and rainfall characteristics;
168 and (iii) compare calibrated model infiltration parameter values with the previous
169 field measurements of K_{sat} by Zhang et al. (2019a) to assess the degree of possible
170 under-estimation of the latter at the catchment scale.

171

172 **2 Materials and methods**

173 **2.1 Study area**

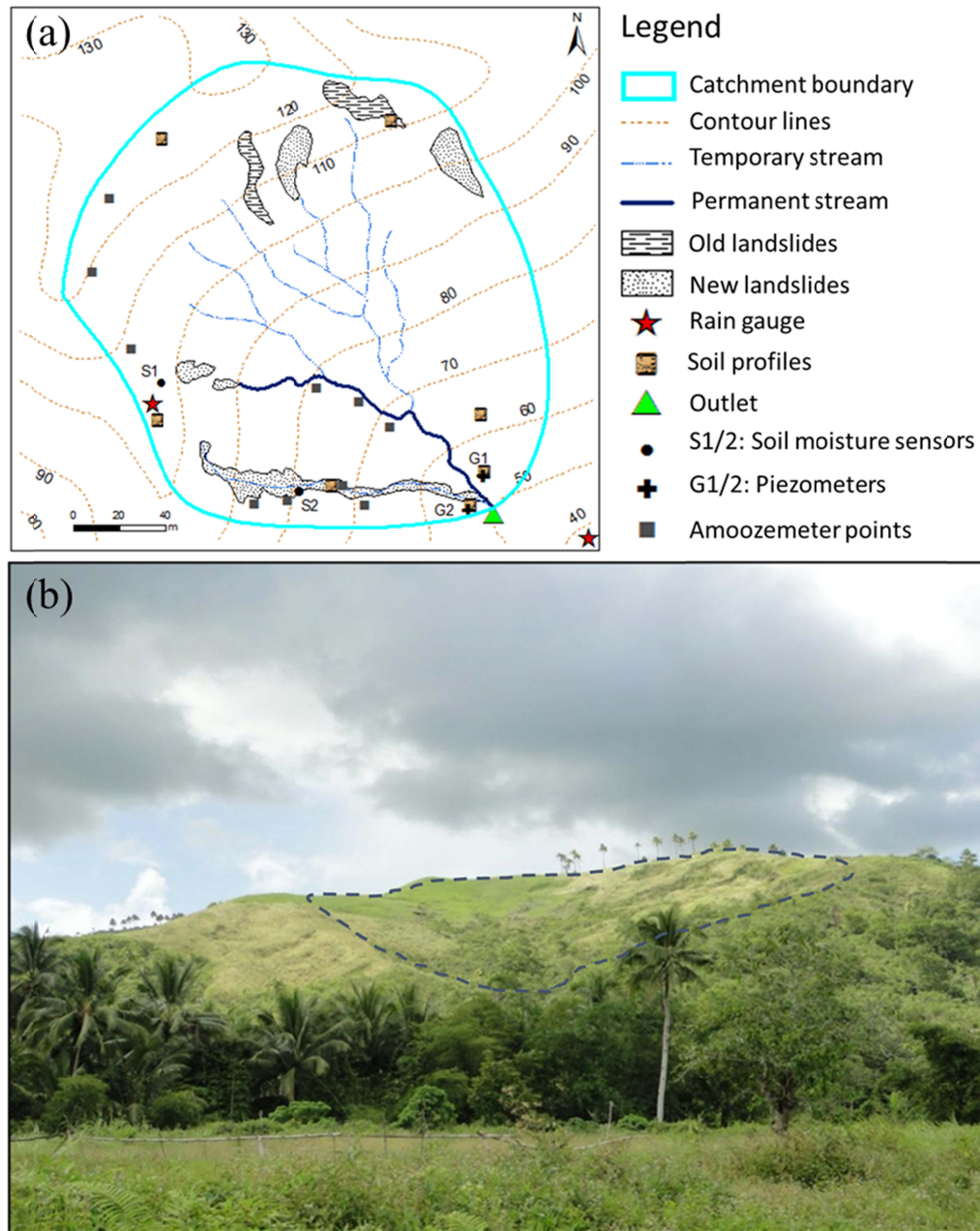
174 The south-facing 3.2-ha Basper catchment (11°15'28" N; 124°57'22" E) is located 14
175 km west of Tacloban, the capital of Leyte Island. Elevations range from 50–135 m
176 a.s.l. The climate is tropical ever-wet (Köppen-type Af) with a mean annual rainfall at
177 Tacloban Airport (1977–2012) of 2,660 mm (range: 1,435–4,790 mm), distributed
178 over 195 rain days (with ≥ 0.5 mm of rain each) on average per year. There is no
179 clear dry season, but average monthly rainfall totals are distinctly higher (>350 mm
180 mo^{-1}) between November and January than for April–May (>100 mm mo^{-1}).
181 Typhoons and tropical storms can bring large amounts of rain and supply roughly
182 one-third of the annual rainfall in the region (Cinco et al., 2016). Between 1977 and
183 2011, ~50% of all rain days at Tacloban Airport received less than 5 mm of rain.
184 Considering only events with ≥ 5 mm of rain, 64% of storms were 5–20 mm in size,
185 whereas 10% and 2.5% of events were larger than 50 and 100 mm, respectively. The
186 median 5-, 15-, 30-, and 60-min rainfall intensities measured at Basper during 99

187 events with at least 5 mm of rain between June 2013 and May 2014 were 3.2, 2.1, 1.5
188 and 1.0 mm h⁻¹, respectively. Corresponding 95th-percentile intensities were 34, 22,
189 18, and 12 mm h⁻¹.

190 The upper slopes are straight to slightly concave, while foot-slopes generally steepen
191 towards the stream. Landslides are a prominent feature and made up 3.4% of the
192 catchment area at the time of the investigation (Zhang et al., 2018a; Figure 1). The
193 vegetation consists of *cogon* grass (*Imperata cylindrica*) on the ridges and upper
194 slopes, with additional sedge (*Cyperus* sp.) in less well-drained parts. The mid-slope
195 parts have a mixture of *Saccharum spontaneum* grass and low shrub (<1.5 m, mostly
196 *Melastoma* and *Chromolaena*), while shrubs and young trees (<3 m, mostly
197 *Neonauclea* and *Leukosyke*) are common on the lower slopes. Although regularly
198 burned in the past, the area did not experience fire after 2003 and young regenerating
199 forest occupied an estimated 4,500 m² (~14%) in the central portion of the catchment
200 at the time of the study (Figure 1).

201 Eutric Cambisols of predominantly clay loam texture, grading to a sandy clay loam
202 below 90 cm depth, overlay the gabbro bedrock. Soil organic carbon content, porosity
203 and drainable pore space decline with depth, while median bulk densities increase
204 with depth in the top 40 cm (Zhang et al., 2019a). The median (\pm median absolute
205 deviation, MAD) steady-state surface infiltration rate (determined using a portable
206 double-ring infiltrometer with inner and outer ring diameters of 15 and 21 cm) was
207 2.1 ± 0.7 mm h⁻¹ ($n = 13$). The median near-surface K_{sat} (<10 cm depth) obtained from
208 small cores (laboratory permeameter) was 1.7 ± 1.6 mm h⁻¹ ($n = 27$). The median K_{sat}
209 at ~20 cm depth as derived with a constant-head well permeameter was 2.7 ± 2.2 mm
210 h⁻¹ (Amoozegar, 1989; $n = 20$; see Zhang et al. (2019a) for details).

211



213
214

219 **Figure 1.** Basper micro-catchment. (a) Map showing the drainage network, and
220 locations of landslides, hydrological instrumentation, soil profiles (core sampling and
221 double-ring infiltration sites), and soil hydraulic conductivity measurements using
222 well permeametry. (b) Photo showing the land cover. The broken line indicates the
223 catchment boundary. Photo credit: Jun Zhang.

219 **2.2 Methods**

220 **2.2.1 Hydrological monitoring**

221 For this study, we used measurements of rainfall, streamflow, soil water content and
222 foot-slope groundwater levels taken between 3 June and 7 November 2013. These
223 measurements represent the conditions prior to the major disturbance to vegetation
224 and soils by Typhoon Haiyan on 8 November 2013 (Zhang et al., 2018a).

225 *Rainfall* (P) was measured using two Onset Computer Corporation RG3 tipping-
226 bucket rain gauges (0.25 mm per tip, confirmed by manual calibration) connected to a
227 HOBO Pendant event data-logger. One gauge was located in the open near the
228 catchment outlet and the other on the upper western ridge (Figure 1a). A standard
229 manual rain gauge (100 cm² orifice) was placed next to each of the recording gauges
230 and read every morning as a check.

231 *Streamflow* (Q) was measured using a sharp-crested compound weir consisting of a
232 0.55 m high 90° V-notch and a horizontal beam extending 0.5 m to each side from the
233 edge of the V-notch (Zhang et al., 2018a). Water pressure was measured at five-
234 minute intervals using a HOBO U20L04 logger and corrected for atmospheric
235 pressure, which was measured by a similar device in a hut located ~100 m from the
236 weir. The standard V-notch weir equation (Bos, 1989) was checked through
237 volumetric discharge measurements below 4.4 l s⁻¹ (staff heights < 0.3 m), and Price
238 Type-AA current-meter measurements at stages up to 0.55 m. Water levels exceeded
239 the shoulder of the V-notch for ~1.3% of the total duration of the 30 selected storm
240 events (Section 2.2.2), representing ~33% of the corresponding total storm runoff
241 amount. For these conditions the Bergmann compound weir equation as given by
242 USBR (1997) was used to calculate the streamflow.

243 *Volumetric soil moisture content* (θ) and *shallow groundwater levels* were monitored
244 at different sites within the catchment (Figure 1a; Zhang et al., 2018a). The present
245 analysis only used soil moisture data from site S2 (*Saccharum* grassland at mid-slope
246 position) and shallow groundwater levels as measured at piezometer site G1 (left
247 bank, 0.9 m deep; Figure 1a). Soil moisture at S2 was measured at five-minute
248 intervals using simplified Time Domain Reflectometry (TDR) sensors (MP-306, ICT

249 International, Australia) installed at 0.1, 0.2, 0.4, 0.6, 0.8, and 1.1 m below the
250 surface, and connected to an ICT International Microvolt data-logger. Water levels in
251 piezometer G1 were also measured at five-minute intervals using a HOBO U20L04
252 logger.

253

254 **2.2.2 Stormflow separation and event selection**

255 To separate stormflow (Q_q) from baseflow (Q_b), the constant-slope method of Hewlett
256 and Hibbert (1967) was applied to the streamflow record for each event prior to
257 Typhoon Haiyan (3 June–7 November 2013). The following criteria were used to
258 define the start of each ‘stormflow event’: (i) total rainfall ≥ 5 mm; and (ii) the event
259 was preceded by a rain-free period ≥ 6 h. For the end of an event, a threshold value
260 of 0.005 mm per five minutes (0.06 mm h⁻¹ equivalent) was used. Furthermore, we
261 only included events for which the five-minute rainfall- and streamflow
262 measurements were complete (*i.e.*, no data gaps). Lastly, events for which $> 10\%$ of
263 the stormflow could have been generated by precipitation falling directly onto the
264 perennial stretch of the stream (~ 90 m² or 0.28% of the total catchment area; Figure
265 1a) were excluded. Thus, only events with a minimum hillslope runoff contribution $>$
266 90% were considered. Application of the above criteria yielded 30 stormflow events
267 for comparative testing of the Spatially Variable and Green–Ampt infiltration models.

268

269 **2.2.3 Likelihood of an overland flow dominated system as inferred from the** 270 **transit time of the rainfall-to-streamflow wave propagation**

271 The extremely low sub-soil K_{sat} -values determined in the field (Zhang et al., 2019a),
272 the high electric conductivity of foot-slope groundwater and pipe flow (~ 270 $\mu\text{S cm}^{-1}$)
273 but strong dilution of streamflow during times of stormflow (Zhang et al., 2018a; Van
274 Meerveld et al., 2019), and high event-water contributions to stormflow (Van
275 Meerveld et al., 2019) all suggest that runoff generation in the Basper catchment is
276 dominated by IOF. But before comparing the performance of the GA and SVI models
277 for the prediction of catchment-wide overland flow generation, we investigated
278 whether the selected storm runoff events were more likely to be generated primarily

279 by IOF than return flow and saturation overland flow (SOF) (*cf.* Dunne & Black,
280 1970; Lapidés et al., 2022) in more detail. Using a data-based mechanistic modeling
281 approach, the rainfall-generated streamflow response time was compared to that of the
282 groundwater level in piezometer G1 in the riparian zone that is influenced by lateral
283 subsurface flow. To facilitate the comparison, the observed piezometer water levels
284 were converted to pore-water depth equivalents by multiplying the water levels times
285 the measured soil porosity (Zhang et al., 2019a). The response times (strictly
286 speaking, of the celerities, not of the velocities of the water particles), were identified
287 from optimal Transfer Function (TF) models using the Nash-Sutcliffe model
288 efficiency (NSE; Nash & Sutcliffe, 1970) and a heuristic measure that helps avoid
289 selection of over-parameterised models (the Young Information Criterion; Young,
290 2001) as selection criteria. A discrete-time, rather than continuous-time, transfer
291 function identification algorithm was used (Chappell et al., 1999) to account for the
292 presence of occasional short breaks in the observed streamflow record. This
293 algorithm, RIVID, is part of the CAPTAIN Toolbox for Matlab (Taylor et al., 2007).
294 A wide range of model structures were evaluated covering first- to third-order models,
295 with pure time delays ranging from zero to 30x the five-minute time-steps, and
296 various non-linearity transformations, including the established Store–Surrogate
297 (Chappell et al., 1999) and Bedford–Ouse approaches (Chappell et al., 2006).
298 The modeling identified time constants of first-order (*i.e.*, single pathway) models of
299 the rainfall-streamflow response that varied between 9–15 min, depending on the
300 event. These times are much smaller (*i.e.*, the response is much faster) than for the
301 cyclone-affected South Creek basin in Queensland, where hillside SOF is important
302 (Chappell et al., 2012), but comparable to those derived for overland flow plots (*e.g.*,
303 Chappell et al., 2006). This suggests a dominance of IOF at Basper. Further, the
304 subsurface response to rainfall in the riparian zone at Basper (*i.e.*, foot-slope
305 groundwater levels) was 9–70 h and thus much slower than the streamflow response
306 to rainfall (9–15 min), again pointing to IOF as the main mechanism for stormflow
307 generation (see examples in Supporting Information S1).

308

309 **2.2.4 Infiltration models**

310 Two models of contrasting complexity were used to quantify the infiltration process
311 and to derive the associated amounts of excess rainfall (r_e). However, an identical
312 runoff routing algorithm was employed in both cases for subsequent comparison with
313 the observed storm runoff hydrographs at the catchment outlet.

314 The first model is based on the Green–Ampt (GA) equation, in which the infiltration
315 capacity (i_c) is expressed as a function of the cumulative infiltration amount, F (in
316 mm) as:

$$317 \quad i_c = K_e \left(1 + \frac{\psi_m}{F} \right) \quad (1)$$

318 where K_e (mm h^{-1}) can be regarded as the ‘effective’ saturated hydraulic conductivity
319 of the surface soil, and ψ_m (mm) as the ‘effective’ matric potential at the wetting front
320 across the catchment. An application of the GA equation for a rainfall event of
321 constant intensity was developed by Mein and Larsen (1973) and for an event of
322 varying intensity by Chu (1978). Computational procedures are described in detail by
323 Chow et al. (1988). Briefly, for each time interval j , given a rainfall intensity p , and a
324 cumulative infiltration F at the beginning of the interval, there are three possible
325 scenarios for the actual rate of excess rainfall (r_e): (i) $p < i_c$, and $r_e = 0$ throughout the
326 interval; (ii) ponding condition, *i.e.* $i_c = p$, is met at some point during the time
327 interval; or (iii) ponding has occurred and p exceeds i_c throughout the interval, hence
328 $r_e = p - i_c$. In each of the three cases, F is updated to the end of the time interval.

329 The second model was SVI (Yu et al., 1997a), which conceptualizes overland flow
330 generation during two distinct phases. At the start of an event, i_c is typically much
331 larger than p , and an initial abstraction, F_0 (in mm) is used to represent the amount of
332 infiltration prior to the commencement of excess rainfall. In other words, r_e is zero at
333 this stage – irrespective of rainfall intensity, as long as cumulative rainfall is less than
334 F_0 :

$$335 \quad r_j = 0, \text{ when } \sum_{i=1}^j p_i \leq F_0 \quad (2)$$

336

337 Once cumulative rainfall has exceeded F_0 , the actual rate of infiltration, i_a is modeled
338 as a function of the rainfall intensity and a spatially averaged maximum infiltration
339 rate, I_m (both in mm h^{-1}). The main assumption behind the SVI model is that i_c varies

340 in space according to an exponential distribution that involves I_m as a single parameter
 341 (Yu et al., 1997a; cf. Hawkins & Cundy, 1987; Supplementary Figure S1).

342 It can be shown (Yu et al., 1997a) that:

343

$$344 \quad i_a = I_m(1 - e^{-p/I_m}) \quad (3)$$

345

346 Application of either SVI or GA leads to a time series of excess rainfall on hillslopes
 347 as the difference between rainfall intensity and the modeled rate of infiltration:

348

$$349 \quad r_e = p - i_a \quad (4)$$

350

351 To take the rain falling directly on the surface of the perennial stream (*i.e.*, channel
 352 precipitation; see Section 2.2.2 above for rationale) into account, the total excess
 353 rainfall, r^* was expressed as the area-weighted sum of rainfall excess over the stream
 354 channel and that over the hillslopes:

355

$$356 \quad r^* = (1 - f_w)r_e + f_w p \quad (5)$$

357

358 where f_w is the fractional area of the perennial stream channel (in this case: 0.28%).

359

360 Regardless of the infiltration model used, for each time interval, j , with excess rainfall
 361 computed using equations (4) and (5), r^* is routed to the catchment outlet using a
 362 simple kinematic wave approximation:

363

$$364 \quad Q_j = \alpha Q_{j-1} + (1 - \alpha)r_j \quad (6)$$

365 where Q_j is the stormflow rate at the catchment outlet for time interval j (in mm h^{-1}).

366 The routing parameter, α , is related to the catchment lag time, T (in hours), and the
 367 adopted time interval for the rainfall and storm runoff observations, Δt as follows (Yu
 368 et al., 1997a):

369

$$370 \quad \alpha = \begin{cases} T/(T + \Delta t) & T \leq \Delta t/2 \\ (2T - \Delta t)/(2T + \Delta t) & T > \Delta t/2 \end{cases} \quad (7)$$

371

372 The advantage of using Equation (6) for routing is the guaranteed numerical stability,
373 irrespective of the magnitude of T relative to Δt .

374

375 **2.2.5 Model calibration and evaluation**

376 The parameters for the two models were optimized by minimizing the sum of squared
377 errors (SSE) between the observed and modeled stormflow using the Levenberg-
378 Marquardt algorithm (Marquardt, 1963):

379

$$380 \quad \min SSE = \sum_{j=1}^N (Q_j - \hat{Q}_j)^2 \quad (8)$$

381

382 where \hat{Q}_j and Q_j are the modeled and observed stormflow rates, respectively (in mm
383 h^{-1}), and N is the total number of time intervals for the event. Model parameters were
384 calibrated for each individual event to account for temporally varying infiltration
385 rates, resulting in 30 parameter sets (one for each event) for each of the two
386 infiltration models. The two infiltration models were fully integrated with the
387 Parameter ESTimation Software (PEST++) for efficient parameter estimation (White
388 et al., 2020).

389

390 To evaluate model performance, the Nash-Sutcliffe efficiency was calculated for each
391 of the 30 individual storm runoff hydrographs. Further, we computed the Sum of
392 Squared Errors, percent bias (PBIAS; Gupta et al., 1999), and the ratio between the
393 RMSE of the observations and their standard deviation (RSR; Legates & McCabe,
394 1999) for each event. Although the two infiltration models were applied primarily to
395 test their ability to predict storm hydrographs at five-minute intervals, model
396 performance was also examined in terms of stormflow amount (Q_q) and peak runoff
397 rate (Q_p) for individual events.

398

399 **2.2.6 Relations between infiltration model parameters and event characteristics**

400 The calibrated infiltration model parameters were related to event rainfall
401 characteristics to examine whether – and to what extent – the model parameters were
402 affected by rainfall characteristics and antecedent conditions. The main event
403 characteristics used in the Spearman rank correlation analysis were the peak intensity
404 and the maximum rainfall intensities during 15 and 30 min. The main indicators of

405 antecedent wetness conditions were the three-day antecedent precipitation index
406 (API₃) and the volumetric water content in the top 10 cm of the soil at mid-slope
407 position (SWC₁₀). The Antecedent Precipitation Index (API) is a measure of
408 catchment wetness based on the rainfall that occurred over preceding days and was
409 calculated as:

$$410 \quad \quad \quad API = \sum_{n=1}^N P_n k^n \quad (9)$$

411 where P_n is the precipitation during the n^{th} day preceding the day for which the API is
412 calculated, and k is a decay constant. Given the small size and comparatively shallow
413 soils of the study catchment, we decided to use a three-day antecedent precipitation
414 index (API₃) using a k value of 0.80 (Shaw et al., 2010).

415

416 **2.2.7 Comparison of hydraulic model parameters with field measurements**

417 The point-measured K_{sat} data from Zhang et al. (2019a) were compared directly with
418 the model-calibrated values of near-surface K_{sat} (*i.e.*, K_c in GA and I_m in SVI). In
419 addition, the *distributions* of the two data series were compared, noting that the
420 underlying idea of the SVI model is that the spatial variation in infiltration capacity i_c
421 can be described by an exponential distribution of the maximum infiltration capacity
422 I_m according to Equation (3) (Yu et al., 1997a). To approximate an overall distribution
423 of i_c for the Basper catchment, the 30 event-based values of I_m were each inserted
424 separately into Equation (3) to derive the corresponding distributions of i_c . The
425 average distribution for all 30 events was regarded as representing the overall spatial
426 distribution of i_c across the catchment. Because differences in mean field K_{sat} based on
427 portable-ring infiltrometry ($n = 13$), near-surface well permeametry ($n = 20$), and
428 laboratory permeametry on small cores ($n = 27$) were not statistically significant (p-
429 value > 0.35), all data were bulked ($n = 60$).

430

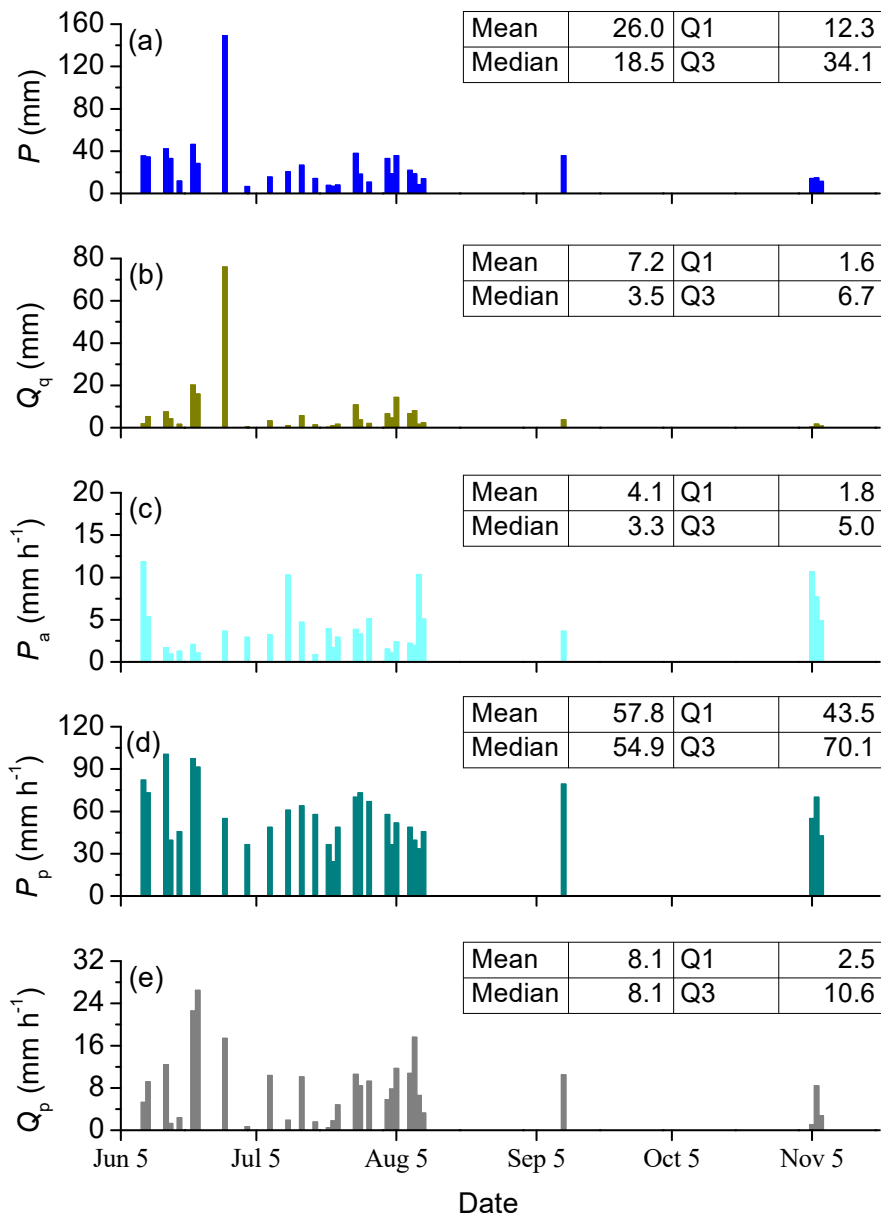
431 **3 Results**

432 **3.1 Characteristics of selected storm events**

433 Rainfall amounts for the 30 events ranged from 6.6 to 149 mm, with a mean of 26 mm
434 (median 18.5 mm; Figure 2). Event total stormflow at the catchment outlet varied

435 from 0.3 mm to 76 mm, averaging 7.2 mm (median 3.5 mm), while stormflow runoff
436 coefficients (Q_q/P) ranged from 3–56%, averaging 21% (median 18%). Collectively,
437 these events represented ~66% of the total rainfall during the 3 June–7 November
438 2013 study period (1,187 mm) and ~92% of the total storm runoff (235 mm; Zhang et
439 al., 2018a). Event duration (defined as the time between the initial rise in discharge
440 and the stormflow cut-off point; Section 2.2.2) varied from 0.8 to 40.8 h, averaging
441 10.4 h (median 6.0 h). Event-averaged rainfall intensity (4.3 mm h⁻¹; median 3.3 mm
442 h⁻¹) was approximately an order of magnitude smaller than the five-minute peak
443 rainfall intensity (average: 58 mm h⁻¹, median 55 mm h⁻¹; Figure 2). Based on their
444 Q3/Q1-ratios (*i.e.*, between the third and first quantiles), rainfall amounts and peak
445 rainfall intensities varied less between events than stormflow amounts and peak
446 runoff rates (Figure 2).

447



448

449 **Figure 2.** Time series showing the basic characteristics of the 30 examined runoff
 450 events at Basper catchment between 6 June and 7 November 2013: **(a)** rainfall (P ,
 451 mm), **(b)** total stormflow (Q_q , mm), **(c)** average rainfall intensity (P_a , mm h⁻¹), **(d)**
 452 peak rainfall intensity (P_p , mm h⁻¹) and **(e)** peak stormflow rate (Q_p , mm h⁻¹). Insets
 453 list the means, medians, as well as the first (Q1) and third (Q3) quantiles for the
 454 respective variables.

455

456

457

458

459 **3.2 Comparative infiltration model performance**

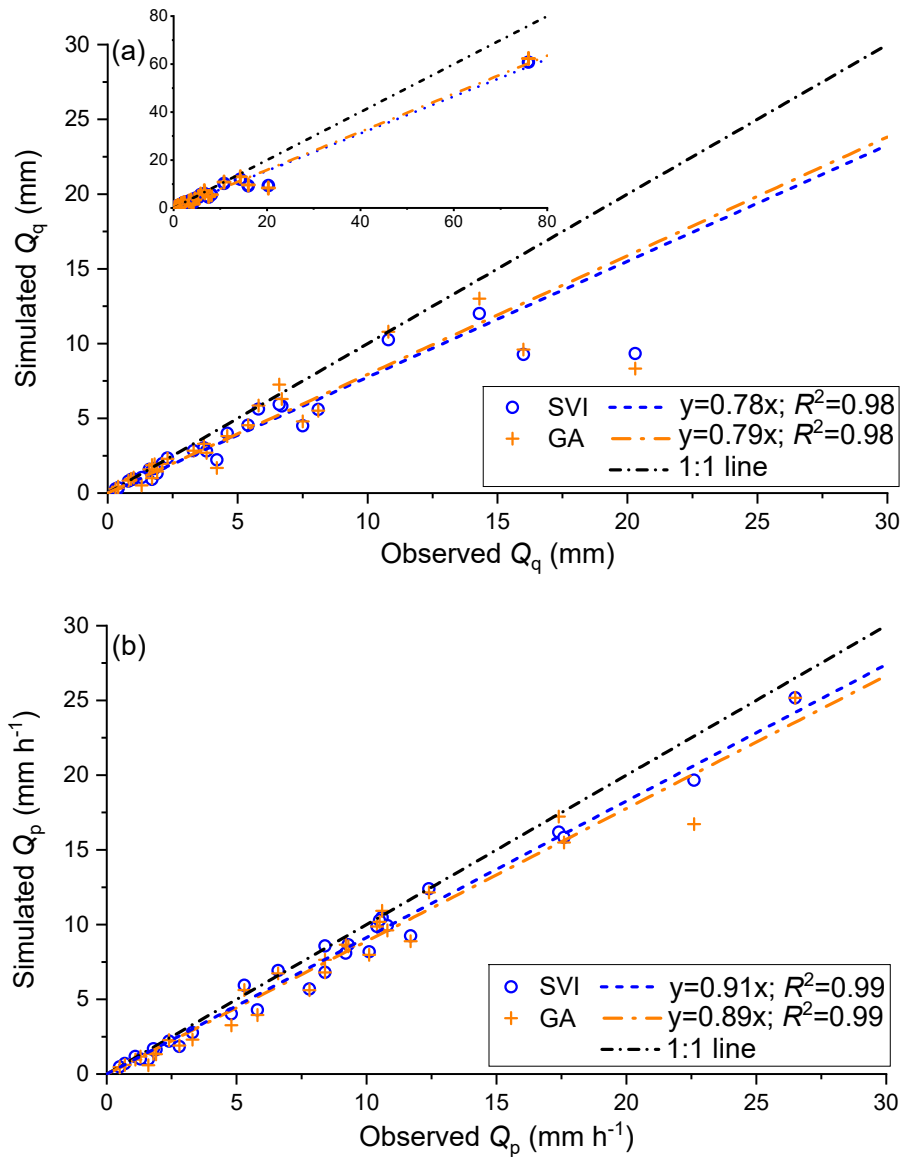
460 GA and SVI could be calibrated equally well to simulate event-based Q_q and Q_p , with
 461 simulated Q_q and Q_p being in good agreement with observed values (R^2 -values of 0.98
 462 and 0.99, respectively, regardless of the model used; Figure 3). Nevertheless, the
 463 median Q_q tended to be under-estimated by about 10% (GA) to 14% (SVI; Table 1)
 464 and by 21–22% for larger events (based on the slopes of the regression lines in Figure
 465 3a). Peak runoff rates were under-estimated by about 8–12% (Figure 3b; Table 1).
 466 However, based on the higher NSE- and lower RSR-values, SVI performed slightly
 467 better than GA in terms of simulating event-based stormflow (Table 1).

468

469 **Table 1.** Model performance of SVI and GA for the prediction of storm runoff totals
 470 (Q_q) and peak runoff rates (Q_p) for the 30 examined storm events.
 471

Model	Evaluation	Min	Q1	Median	Q3	Max
SVI	SSE ¹ (Calibration)	0.04	1.6	4.6	23	418
	NSE ²	0.57	0.84	0.92	0.95	0.99
	PBIAS ³ $_Q_q$	-2	6	14	26	54
	PBIAS ³ $_Q_p$	-12	2.5	8	18	39
	RSR ⁴	0.10	0.23	0.28	0.40	0.66
GA	SSE ¹ (Calibration)	0.03	2.1	6.8	29.5	589
	NSE ²	0.12	0.74	0.88	0.94	0.99
	PBIAS ³ $_Q_q$	-10	-0.8	10	28	60
	PBIAS ³ $_Q_p$	-6	5	11.5	26	63
	RSR ⁴	0.10	0.25	0.35	0.51	0.94

472 ¹Sum of squared errors; ²Nash-Sutcliffe efficiency; ³Per cent bias; ⁴Ratio between the RMSE and the
 473 standard deviation of the observations

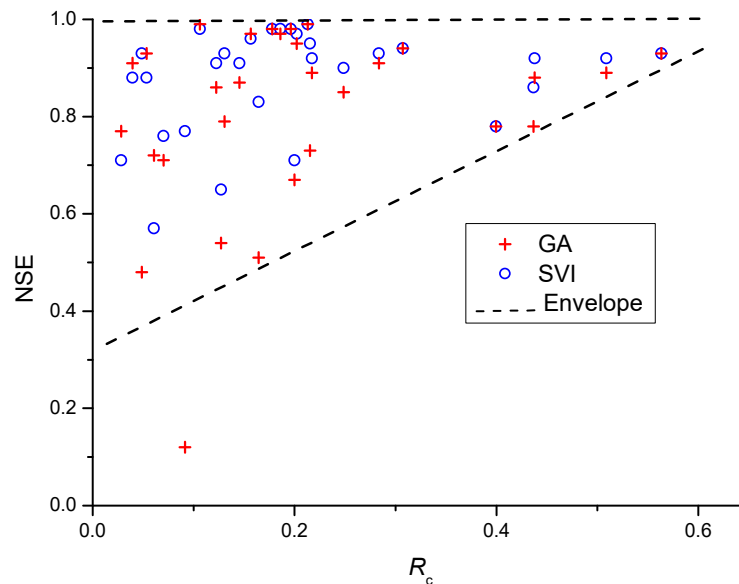


474
 475 **Figure 3.** Comparison of the observed and modeled (a) stormflow totals (Q_q , mm)
 476 and (b) peak runoff rates (Q_p , mm h⁻¹) for the 30 examined runoff events. The models
 477 were calibrated for each individual event by minimizing the sum of squared errors.

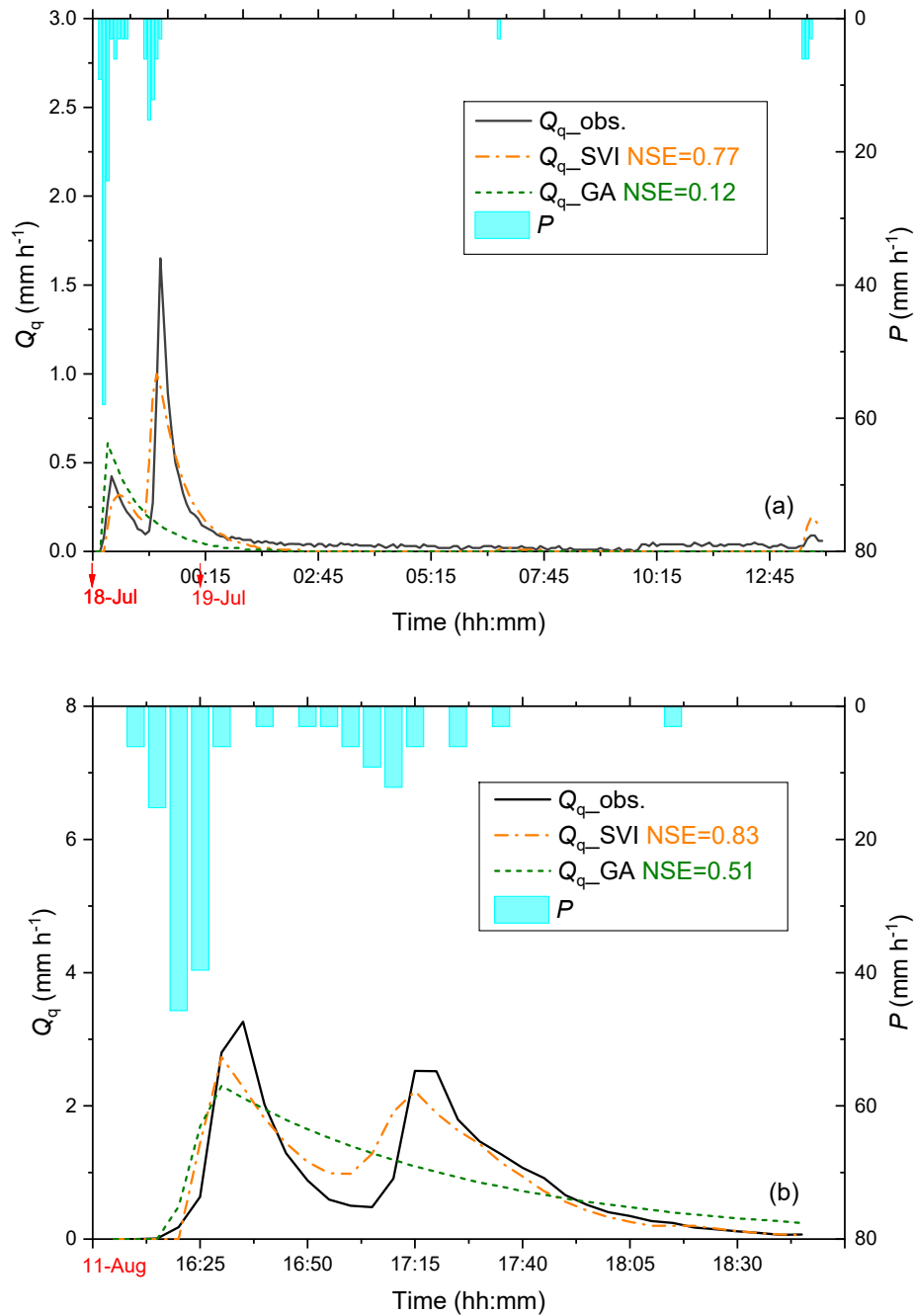
478

479 Figure 4 shows the model performance in terms of the NSE-values derived for
 480 individual events *versus* corresponding stormflow runoff coefficients ($R_c = Q_q/P$). As
 481 indicated by the enveloping line, both models captured events with higher runoff
 482 coefficients better than events with lower R_c , for which low NSE-values suggested a

483 poor model fit (Figure 4). Overall, SVI outperformed GA in terms of its ability to
 484 reproduce event-based hydrographs, with average NSE-values for all 30 events of
 485 0.88 for SVI *versus* 0.81 for GA (difference significant at a p-value < 0.05). Out of 13
 486 events with $R_c \leq 0.16$, three were captured poorly by GA (*i.e.*, $NSE \leq 0.50$) *versus*
 487 none for SVI (Figure 4). Simulations for two specific events with multiple runoff
 488 peaks are presented in Figure 5 to illustrate the difference in model performance for
 489 complex events. GA missed the second peak of the hydrograph entirely for both
 490 events, whereas SVI was capable of simulating all peaks despite a certain degree of
 491 under-estimation. A similar pattern was noted for the events with a particularly high
 492 rainfall intensity at the beginning of the storm, which caused GA-modeled stormflow
 493 to occur earlier than observed (see Supplementary Figures S2a and S2b).



494
 495 **Figure 4.** Relationship between stormflow runoff coefficient (R_c) and the Nash–
 496 Sutcliffe model efficiency as a measure of model performance for the GA and SVI
 497 models for the 30 examined events.



498

499 **Figure 5.** Observed and simulated stormflow hydrographs for two example events
 500 with two runoff peaks for which SVI outperformed GA due to the latter's failure to
 501 simulate the consecutive peaks: **(a)** the 14 mm event of 18–19 July 2013, with a
 502 stormflow runoff coefficient (R_c) of 10%, and **(b)** the 14 mm event of 11 August
 503 2013, with R_c of 17%.

504 **3.3 Infiltration model parameter variability**

505 The optimized values for the three parameters for each infiltration model (F_0 and I_m
 506 for SVI; K_e and ψ_m for GA, plus lag time T in both models) are summarized in Table
 507 2. Coefficients of variation (CV) were larger for I_m and K_e compared to the other
 508 parameters. The comparison of the ratio of the third and first quantiles (Q3/Q1)
 509 suggests that K_e and lag time T in GA varied more from event to event than I_m and T
 510 in SVI. Mean lag times for the two infiltration models did not differ significantly (p-
 511 value = 0.19).

512

513 **Table 2.** Variability of the optimized infiltration model parameters for the 30
 514 examined events: F_0 = initial abstraction (mm), I_m = spatially averaged maximum
 515 infiltration capacity (mm h⁻¹), T = lag time (min), K_e = ‘effective’ final infiltration rate
 516 (mm h⁻¹), and ψ_m = matric potential at the wetting front (mm). Q1, Q2 and Q3 indicate
 517 the 1st, 2nd and 3rd quantiles of the respective parameter values. CV denotes the
 518 coefficient of variation and C_s the skewness.

519

Model	Model parameter	Q1	Q2	Q3	Mean	CV	Q3/Q1	C_s
SVI	F_0	5.1	7.0	9.4	7.9	0.5	1.8	1.2
	I_m	22.9	31.6	48.7	47.8	1.1	2.1	2.5
	T	8.6	14.0	19.9	16.9	0.7	2.3	1.7
GA	K_e	3.1	7.5	11.7	9.4	0.9	3.8	1.3
	ψ_m	21.9	24.6	27.4	27.8	0.7	1.2	1.4
	T	12.0	22.3	32.0	25.9	0.6	2.7	0.8

520

521 The infiltration-related parameters F_0 , I_m and K_e (but not ψ_m) were all positively
 522 affected by rainfall intensity (regardless whether represented by the five-minute peak
 523 intensity P_p , or maximum intensities over 15 or 30 min, P_{15} or P_{30}), whereas the lag
 524 time for either infiltration model was inversely related to rainfall intensity (Table 3).
 525 Furthermore, both F_0 and I_m exhibited significant, negative correlations with SWC_{10}
 526 (Figure 6), but not with API_3 . So did K_e to a lesser extent, but not ψ_m (Table 3).

527

528

529

530

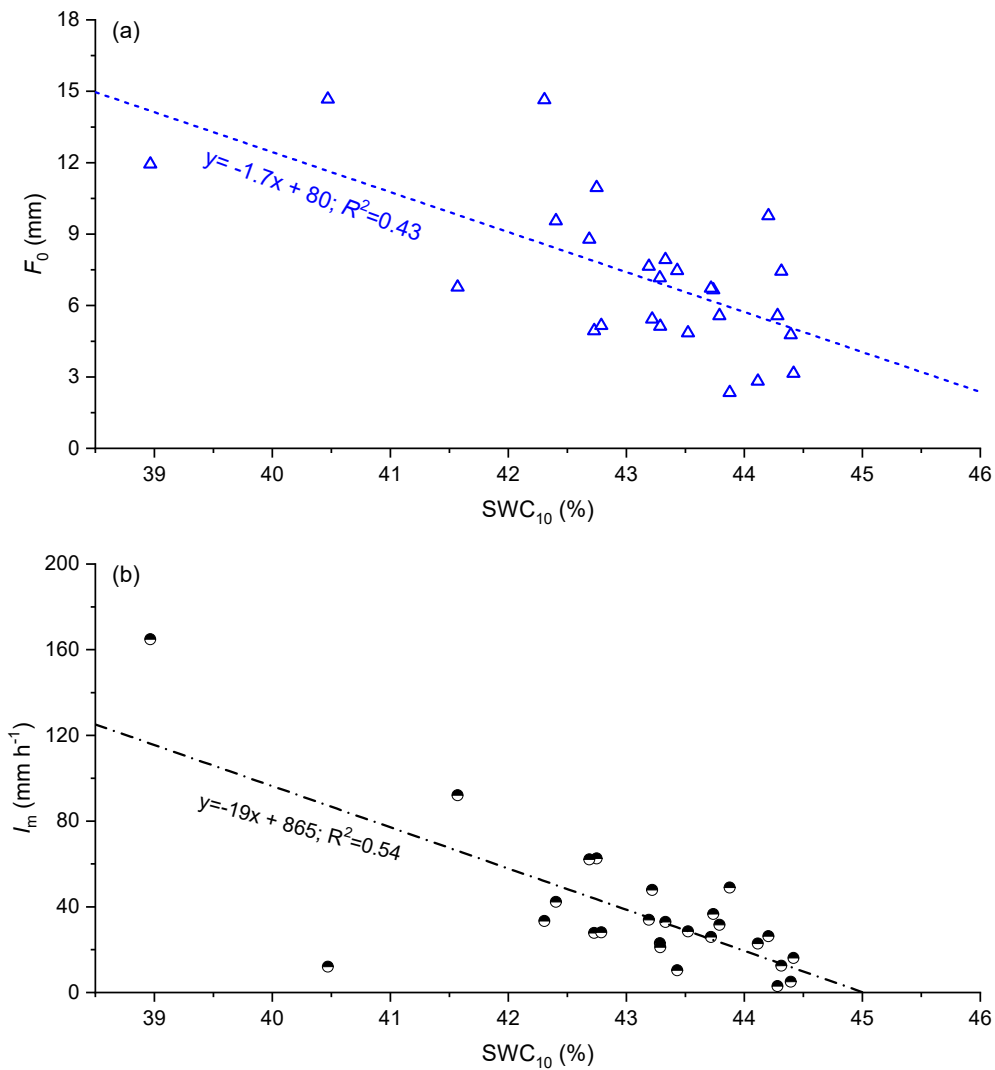
531 **Table 3.** Spearman rank correlation coefficients between the infiltration model
 532 parameters and selected rainfall and catchment wetness characteristics: P = event
 533 precipitation (mm), P_a = average rainfall intensity (mm h⁻¹), P_p , P_{15} and P_{30} = maximum 5-min,
 534 15-min and 30-min rainfall intensities (mm h⁻¹ equivalents), API_3 = three-day antecedent
 535 precipitation index (mm), SWC_{10} , SWC_{30} and SWC_{60} = mid-slope soil water contents (%)
 536 down to 10 cm, 30 cm, and 60 cm depth, respectively. *** indicates p-value < 0.001, ** p-
 537 value < 0.05, * p-value < 0.1.
 538

	P	P_a	P_p	P_{15}	P_{30}	API_3	SWC_{10}	SWC_{30}	SWC_{60}
F_0	0.23	0.34*	0.51***	0.52***	0.46**	-0.13	-0.59***	0.09	0.14
I_m	0.47***	0.22	0.63***	0.63***	0.63***	0.01	-0.57***	0.10	0.21
T_{SVI}	0.03	-0.34*	-0.38**	-0.48***	-0.35*	-0.27	0.11	-0.17	-0.05
K_c	0.53***	0.06	0.74***	0.72***	0.68***	-0.03	-0.48**	-0.16	-0.20
ψ_m	-0.25	0.288	-0.13	-0.11	-0.14	-0.06	-0.01	0.21	0.33
T_{GA}	-0.08	-0.23	-0.36**	-0.45**	-0.37**	-0.39**	0.05	-0.37*	-0.30

539

540 3.4 Stormflow prediction using SVI

541 Because the optimized values of the infiltration-related parameters in SVI (*i.e.*, F_0 and
 542 I_m) varied considerably between events (Table 2), predictions of individual stormflow
 543 hydrographs using average or median parameter values might not be very satisfying
 544 (see example events with wet and dry antecedent conditions in Supplementary Figure
 545 S3). However, both F_0 and I_m were clearly related to the near-surface wetness
 546 condition of the catchment as represented by the moisture content of the top 10 cm of
 547 the soil as measured in mid-slope position (though not by that down to 30 or 60 cm,
 548 nor by API_3 ; Table 3). Hence, the linear relationships between SWC_{10} and F_0 or I_m
 549 shown in Figure 6 were used to estimate the values of F_0 and I_m for each of the 26
 550 events for which SWC_{10} -data were available. For each event, we used the median
 551 value of the lag time ($T = 14.0$ min).

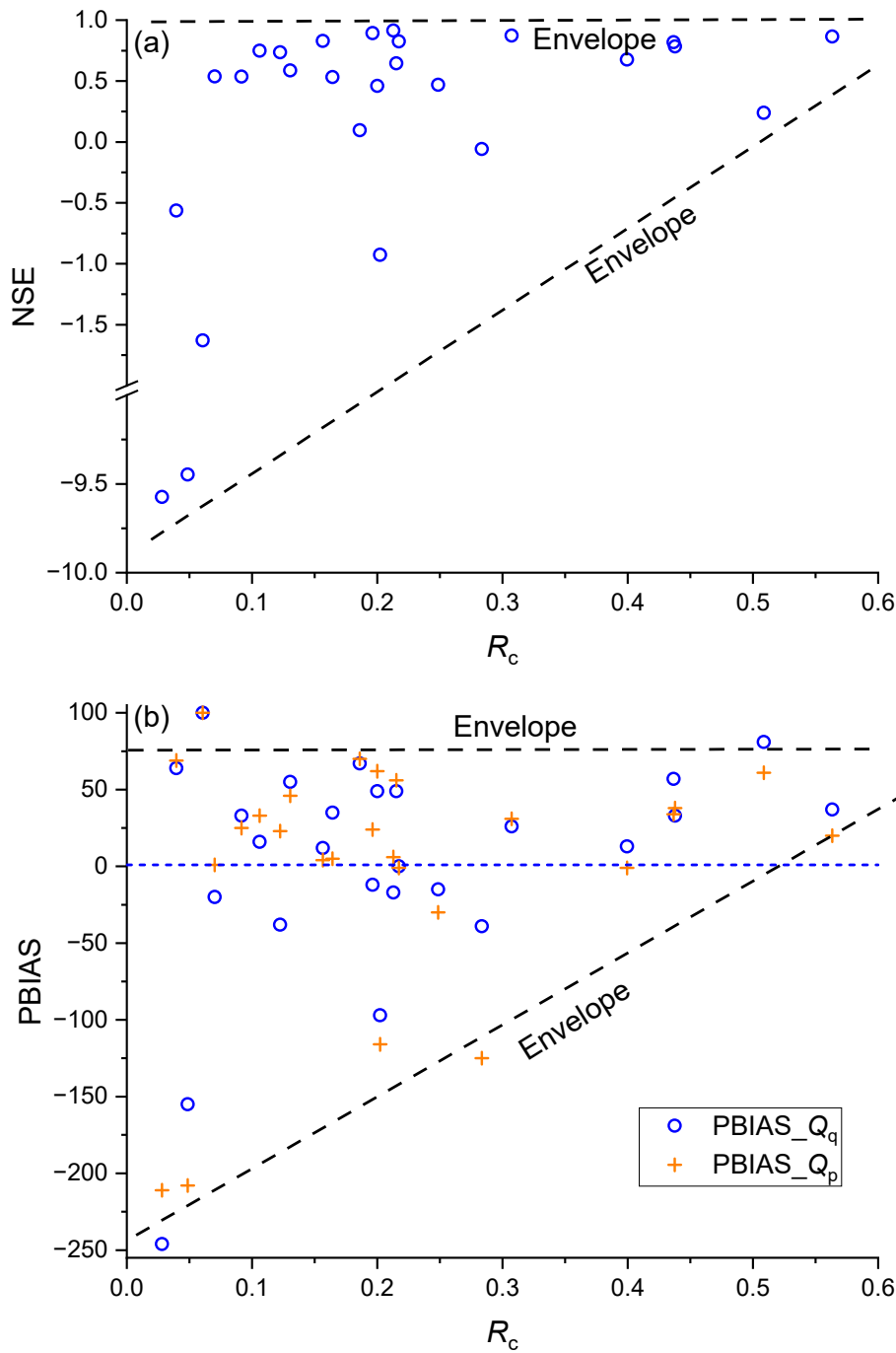


552

553 **Figure 6.** Linear relationships between mid-slope soil water content at 10 cm depth
 554 (SWC_{10}) and the optimized parameter values for (a) spatially average maximum
 555 infiltration rate, I_m , and (b) initial abstraction, F_0 for all 26 runoff events for which
 556 SWC_{10} data were available.

557

558 Satisfactory to good ($NSE > 0.5$) results were obtained for $\sim 70\%$ of the 26 events with
 559 group-based average stormflow runoff coefficients ($R_c = Q_q/P$) larger than ~ 0.15
 560 (Figure 7). However, SVI was less successful at capturing the stormflow hydrographs
 561 of two events with contrasting runoff responses ($NSE\ 0.18\text{--}0.28$; Figure 7).



562

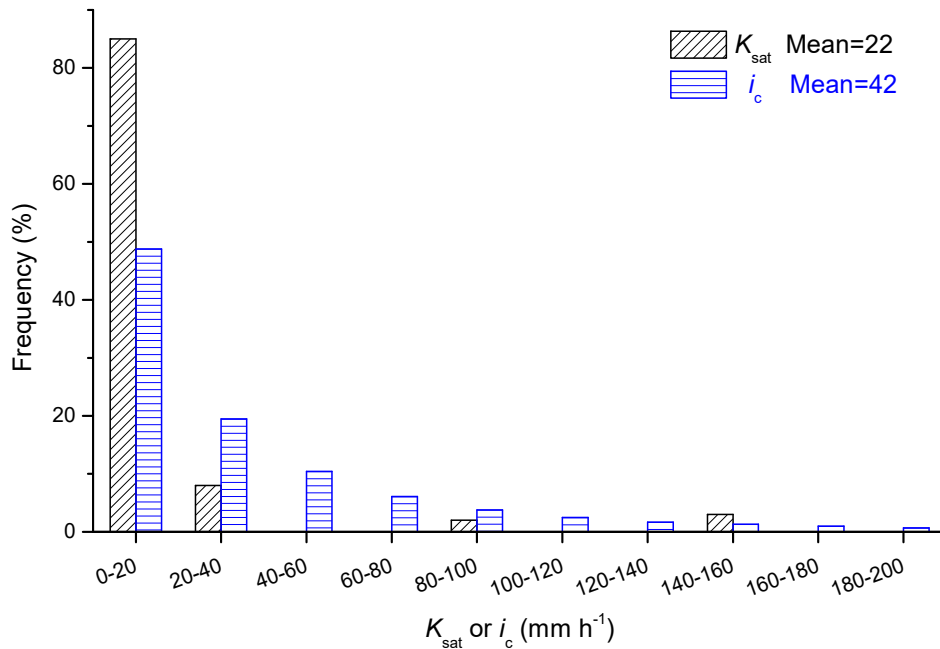
563 **Figure 7.** Relationship between stormflow runoff coefficient (R_c) and (a) the Nash–
 564 Sutcliffe model efficiency (NSE) when the SVI model parameters are based on the
 565 correlation with soil moisture at 10 cm ($F_0 = -1.7 \cdot \text{SWC}_{10} + 80$; $I_m = -19 \cdot \text{SWC}_{10} + 865$,
 566 according to Figure 6); and (b) PBIAS for stormflows (PBIAS $_Q_q$) and peak flow
 567 rates ((PBIAS $_Q_p$).

568 Negative NSE-values were obtained for another six events (23%) representing mostly
569 (but not exclusively) low stormflow runoff coefficients (Figure 7). Two of these six
570 events had comparatively low rainfall amounts (6.6–7.6 mm) and stormflow totals
571 were severely under-estimated by the model. The remaining four events received
572 more substantial amounts of rain (14–38 mm), but SVI over-estimated the amounts of
573 stormflow considerably. Therefore, a comparison was made between calibrated and
574 estimated values of F_0 and I_m ($n = 26$) for different classes of NSE and PBIAS;
575 Supplementary Figure S4). Discrepancies between predicted and calibrated values of
576 F_0 had a significant impact on the model performance (*i.e.*, lower NSE), whereas
577 discrepancies in I_m had a smaller effect (Supplementary Figure S4a). Discrepancies in
578 both F_0 and I_m had an important and significant effect on the simulated amount of
579 stormflow (Supplementary Figure S4b). Higher values of F_0 and I_m led to
580 underestimation of stormflow and *vice versa* (Supplementary Figure S4b).

581

582 **3.5 Comparison of modeled infiltration parameters and measured K_{sat}**

583 The average value for the highly skewed distribution of measured near-surface K_{sat}
584 (22 ± 94 mm h⁻¹ *versus* a median of 2 mm h⁻¹; skewness: 6.4) was roughly half the
585 ~ 42 mm h⁻¹ derived from the averaged exponential distribution of infiltration
586 capacities for the 30 events (skewness: 2; Figure 8). In addition, the shape of the two
587 distributions differed in that comparatively low infiltration capacities (< 20 mm h⁻¹)
588 were encountered far more frequently during the field measurements than implied by
589 the modeling, whereas the reverse applied for intermediate (20–50 mm h⁻¹) and higher
590 infiltration capacities (50–500 mm h⁻¹; Figure 8).



591
592

593 **Figure 8.** Comparison of the spatial distributions of measured K_{sat} ($n = 60$; data from
594 Zhang et al., 2019a) and the modeled infiltration capacity (i_c) based on individual
595 values of I_m for all 30 examined events.

596

597 **4 Discussion**

598 **4.1 Infiltration model performance**

599 With median NSE-values of 0.88 and 0.92, respectively, both GA and SVI performed
600 well for the 30 examined events, with a few notable exceptions. In comparison to SVI,
601 GA is inherently not responsive to changes in rainfall intensity, especially after
602 infiltration reaches steady-state conditions (Yu, 1999). This is likely the main reason
603 why GA was not able to reproduce events with consecutive peaks as well as SVI
604 (Figure 5). Further, high-intensity rain falling on an initially dry soil causes the
605 infiltration capacity to decrease rapidly to values approaching an ‘effective’ K_e (*cf.*
606 Supplementary Figure S1). If subsequent rainfall intensities are less than K_e , this leads
607 to the simulation of low stormflow rates (Figure 5a). Similarly, for events with a
608 particularly high rainfall intensity at the beginning of the storm, the simulation led to

609 large decreases in infiltration capacity within a short period of time, causing GA-
610 modeled stormflow to occur earlier than observed (Supplementary Figure S2).
611 However, SVI did not perform perfectly for events with multiple bursts of rain either.
612 The main reason for this discrepancy lies in the use of constant values for the model
613 parameters for a given event. This assumption is likely to be violated during events
614 with multiple rainfall peaks. An example of this occurred on 3–4 August 2013, when
615 three successive bursts occurred within the event (Supplementary Figure S2c). The
616 first burst occurred on 3 August between 15:20–17:45, the second on 4 August
617 between 00:40–02:45, and the third between 03:20–12:35. The modest runoff peak for
618 the second burst was greatly over-estimated, whereas the larger, third peak was
619 substantially under-estimated (Supplementary Figure S2c). This is likely because the
620 time gap between the first and second bursts (~7 h) was large enough to allow the soil
621 to drain somewhat, thereby re-creating some additional storage opportunity. As a
622 result, part of the rainfall of the second burst was used to fill this additional capacity,
623 causing predicted stormflow rates to be over-estimated. For the third burst, which
624 followed soon after (Supplementary Figure S2c), a lower value of I_m than the applied
625 constant value would have been more appropriate to reflect the wetter soil conditions
626 during this part of the event. Instead, applying a higher, constant I_m throughout the
627 event led to under-estimated stormflow rates for the third burst. A similar under-
628 estimation was also noted for the latter part of the event occurring the following day
629 (Supplementary Figure S2d), where a lower I_m would again have given better results.
630 Both models performed fairly for several events with low stormflow runoff
631 coefficients, even though they were calibrated for these events (*i.e.*, $Q_q/P < 0.10$;
632 Supporting Figures S2e and S2f; *cf.* Figure 4). When applied in predictive mode with
633 F_0 and I_m estimated from mid-slope SWC₁₀ (Figure 6), SVI behaved less than
634 satisfactorily for several other events with (mostly) low runoff coefficients (Figure 7).
635
636
637

638 4.2 Infiltration model parameters: variability and influences

639 Calibrated values for initial abstraction loss (F_0) and spatially averaged maximum
640 infiltration capacity (I_m) in SVI, as well as for the ‘catchment effective’ infiltration
641 capacity (K_e) in GA, varied substantially between the 30 examined events, with
642 overall Q3/Q1-ratios of 1.8, 2.1, and 3.8, respectively (Table 2). As expected on the
643 basis of general infiltration theory (Brutsaert, 2005), all three parameters were
644 negatively correlated with topsoil moisture content (SWC_{10}), albeit not with moisture
645 contents down to greater depths, nor with the three-day antecedent precipitation index
646 (Table 3). Patin et al. (2012) did not find clear relationships between I_m and API per
647 land cover for numerous 1-m² microplots under various land covers in Lao PDR
648 either, but low values were derived at the height of the rainy season and maximum
649 values late in the dry season. In addition, temporal variability in I_m of soils under
650 young fallow vegetation after slash-and-burn cropping (as practiced in the past at
651 Basper; Zhang et al., 2019a) was markedly greater than that for bare soil, upland rice
652 or *Imperata* grassland. Patin et al. (2012) concluded that variations in the water use of
653 (taller) vegetation types between rainfall events affected I_m through modification of
654 soil water contents in more subtle ways than could be captured by a proxy like API
655 with a stationary (*i.e.*, fixed) recession constant (*cf.* Eq. (9)) that does not capture
656 variations in wetness conditions due to differences in evapotranspiration rates. As
657 such, linking infiltration model parameter values to measured topsoil moisture
658 contents is to be preferred (*cf.* Figure 6). In line with the findings of Patin et al.
659 (2012), I_m at Basper also varied seasonally. Calibrated values less than 50 mm h⁻¹
660 were obtained for events during the rainy June–August period, increasing to 75–175
661 mm h⁻¹ during the drier September–November period (Supplementary Figure S5).
662 The presence of a well-developed vegetation cover affects the magnitude of I_m and F_0
663 also in other, indirect ways. Vegetation provides protection of the soil surface against
664 rain drop impact, slaking and crust formation (Wiersum, 1985; Rose et al., 1997;
665 Durán-Zuazo & Rodríguez-Pleguezelo, 2008; Miyata et al., 2009; Lacombe et al.,
666 2018), and promotes soil faunal activity and macropore formation, thereby enhancing

667 infiltration (Blanchart et al., 2004; Shougrakpam et al., 2010; Zwartendijk et al., 2017;
668 Toohey et al., 2018). Indeed, the strongest correlation between I_m and any particular
669 soil characteristic in the Laotian study by Patin et al. (2012) was that with the extent
670 of surface crusting. Hence, comparative median values of I_m for different land-cover
671 types effectively reflected their capacity to prevent crust formation (low for bare soil,
672 high for fallows). Crusting was not studied explicitly at Basper, but the low
673 infiltration capacities recorded by Zhang et al. (2019a) were attributed primarily to
674 erosion during former slash-and-burn cropping phases that exposed the denser sub-
675 soil to the impact of rain drops, as well as a general absence of soil biotic activity and
676 macropores (Quiñones, 2014), and inherent limitations of the K_{sat} measurements (see
677 also discussion below). Repeated cycles of slash-and-burn agriculture can effectively
678 destroy the macropore systems formed during fallow periods (Shougrakpam et al.,
679 2010; Zwartendijk et al., 2017). Pertinently, soil moisture contents at 60 cm depth in
680 the Basper grassland hardly responded to fluctuations in rainfall (Zhang et al., 2018a).
681 Conversely, soil moisture at the same depth beneath a nearby forest responded rapidly
682 to rainfall (Zhang et al., 2018b), suggesting the presence of preferential flow pathways
683 that allowed rapid percolation to deeper layers (Van Meerveld et al., 2019; Zhang et
684 al., 2019a; *cf.* Y. Cheng et al., 2018).

685 In line with the trend noted above for I_m , F_0 can also be expected to be higher for
686 well-vegetated or mulched surfaces than for bare soils (Yu et al., 1997b; Van Dijk &
687 Bruijnzeel, 2004). The limited data available for tropical sites do not suggest that soil
688 texture has a notable influence on the magnitude of F_0 or I_m (in contrast to findings for
689 K_c by Nearing et al., 1996). Increases in soil organic matter content (SOM) tend to
690 have a positive effect, whereas increases in bulk density tend to have a negative effect
691 (Coughlan, 1997; Yu et al., 1997b; Van Dijk & Bruijnzeel, 2004). However, with the
692 possible exception of the relationship between I_m and bulk density ($R^2 = 0.923$, $n = 7$),
693 the predictive capacity of such tentative equations is still low (Supplementary Figure
694 S6) and many more empirical data are required.

695 The currently derived median F_0 (7.6 mm, Table 2) exceeded most of the values
696 reported by Yu et al. (1997b) for various bare agricultural plots in Southeast Asia and
697 Queensland (2.3–6.0 mm), which generally had higher bulk densities and lower SOM
698 than the Basper grass- and shrubland (Coughlan, 1997; Zhang et al., 2019a;
699 Supplementary Figure S6). Higher values of F_0 were obtained at the same sites after
700 application of a surface mulch (~13 mm; Yu et al., 1997b). As such, the interception
701 storage capacity afforded by the tall grasses and shrubs at Basper (and their litter) may
702 well have raised the effective value of F_0 somewhat (*cf.* Leopoldo et al., 1981;
703 Waterloo et al., 1999; Bruijnzeel, 1988). In addition, it cannot be excluded that
704 variations in rainfall intensity at Basper further affected the magnitude of F_0 indirectly
705 through variations in wet canopy evaporation rates between successive storms as
706 observed in a nearby forest by Zhang et al. (2018b). This would not only go some way
707 towards explaining the positive correlations between F_0 and short-term rainfall
708 intensities (P_{15} and P_{30} ; Table 3), but possibly also the discrepancies between SWC₁₀-
709 based estimates of F_0 and calibrated values for certain poorly predicted events
710 (negative NSE; Supplementary Figure S4a).

711

712 **4.3 Difficulty of estimating effective hydraulic conductivity and infiltration**

713 **capacity from point measurements**

714 The median values of the model-based estimates of catchment-wide ‘effective’ (K_e)
715 and ‘maximum’ (I_m) infiltration (7.5 mm h⁻¹ for GA and 31.6 mm h⁻¹ for SVI) were
716 distinctly higher than the field-based measurements of K_{sat} (1.7–2.7 mm h⁻¹,
717 depending on the method used; Zhang et al., 2019a). Also, the SVI-inferred
718 *distribution* of infiltration capacities suggested generally higher values compared to
719 the results obtained by the measurements (Figure 8). However, the measured values
720 were also much lower than the median value reported for similarly textured, non-
721 grazed *Imperata* grassland soils elsewhere in the Palaeo-tropics (35 mm h⁻¹, $n = 8$;
722 range: 15–95 mm h⁻¹; Zhang et al., 2019a; Ghimire et al., 2021). The methods used
723 for measuring near-surface K_{sat} at Basper may have under-estimated actual hydraulic
724 conductivities to some extent – either because of under-sampling of macropores in the
725 case of small cores and small-diameter ring infiltrometry (Davis et al., 1996; Lai &

726 Ren, 2007) or due to smearing of boreholes during augering in the case of well
727 permeametry (Sherlock et al., 2000; Bonell et al., 2010). In addition, it cannot be
728 excluded that somewhat higher values of K_{sat} may have been associated with the
729 denser (less penetrable) parts of the regenerating vegetation in the central part of the
730 catchment, where only a few K_{sat} measurements were conducted (Figure 1a). As such,
731 overall mean catchment-wide K_{sat} may also be higher than inferred from the
732 measurements by Zhang et al. (2019a) due to the spatial bias in field sampling.
733 Furthermore, point-measured K_{sat} -values typically under-estimate the ‘block
734 permeabilities’ of whole hillslopes (Wen & Gomez-Hernandez, 1996; Chappell et al.,
735 1998; Brooks et al., 2004; Pirastru et al., 2017). This under-estimation of block
736 permeability is also seen where statistical distributions of point-measured K_{sat} values
737 are compared directly with ‘effective’ parameter values derived from inversion of
738 catchment models (e.g., Beven, 1989; Blöschl & Sivapalan, 1995; Mertens et al.,
739 2005).

740 Both I_m and K_e are commonly applied to characterize soil infiltration capacity (Yu,
741 2000; Nearing et al., 1996). The relationship between the two is of interest because it
742 allows derivation of modeled I_m (the spatially averaged *maximum* infiltration capacity)
743 from K_e (the ‘effective’ infiltration rate after reaching steady-state conditions; cf.
744 Supporting Figure S1) obtained by inverse means from either IOF (plots) or
745 stormflow (catchments) measurements and GA (e.g., Nearing et al., 1996). In
746 agreement with these definitions, derived values for I_m at Basper (3–259 mm h⁻¹) were
747 higher than those for K_e (1–31 mm h⁻¹). As also reported by Yu (1999) for six
748 different locations in Australia and Southeast Asia, I_m at Basper was positively
749 correlated with K_e . As shown in Supporting Figure S7, the second-order polynomial
750 describing the relation between K_e and I_m for the Basper grassland had an R^2 of 0.45
751 ($n = 30$) compared to $R^2 = 0.80$ ($n = 60$) for the equation derived by Yu (1999).
752 Additional empirical data for different tropical locations are desirable to complement
753 these tentative equations.

754

755 **5 Conclusions**

756 Five-minute rainfall and runoff data collected during 30 events (6.6–149 mm of rain)
757 were used to calibrate two infiltration models of different complexity for the
758 prediction of stormflow responses for a 3.2 ha fire-climax grassland catchment at
759 Basper, Leyte Island (the Philippines). The catchment has soils with very low
760 hydraulic conductivity (K_{sat}) and infiltration-excess overland flow is inferred to be the
761 dominant storm runoff generation mechanism. Landslide scars with low-infiltrability
762 slip surfaces are prominent, covering 3.4% of the area.

763 In the Green–Ampt model (GA), the infiltration rates decline steadily after the start of
764 infiltration, whereas the Spatially Variable Infiltration model (SVI) describes
765 infiltration as a function of short-term fluctuations in rainfall intensity. SVI
766 systematically reproduced the observed stormflow hydrographs better than GA,
767 especially for events with multiple peaks. Calibrated values of the parameters for SVI
768 (notably, spatially averaged maximum infiltration capacity, I_m and initial abstraction,
769 F_0) varied markedly between events, and showed significant negative linear
770 correlations with mid-slope topsoil water content (SWC_{10}) – as did the ‘effective’
771 hydraulic conductivity (K_e) in GA. Using SWC_{10} -based values of I_m and F_0 in SVI
772 produced satisfactory to good ($\text{NSE} > 0.5$) predictive results for ~70% of the
773 examined storms, but failed to reproduce hydrographs for six events (23%) with
774 variable runoff responses, possibly because F_0 was also affected by variations in
775 rainfall interception losses between storms. Deviations between calibrated and
776 SWC_{10} -predicted values of F_0 had a greater impact on predicted stormflow amounts
777 than corresponding deviations in I_m .

778 The median I_m and, to a lesser extent K_e , inferred for the 30 examined events (31.6
779 and 7.5 mm h^{-1} , respectively) were much higher than the median values of near-
780 surface K_{sat} measurements (2–3 mm h^{-1} , depending on method), confirming the
781 previously suspected under-estimation of field-measured K_{sat} in the study catchment.

782 Summarizing, using pre-storm topsoil moisture content and 5-min rainfall intensities
783 as the driving variables to model infiltration with a spatially variable infiltration
784 model resulted in more realistic simulated stormflow responses than the classic

785 Green–Ampt approach or the comparison of rainfall intensities with field-measured
786 K_{sat} to predict stormflow responses at the small catchment scale.

787

788 **Acknowledgements**

789 Financial support for the fieldwork underlying this study from the China Scholarship
790 Council, VU University Amsterdam, and the Australian Council for International
791 Agricultural Research (ACIAR Grant no. ASEM/2010/050) is gratefully
792 acknowledged. The modeling work by Zhuo Cheng was supported by the National
793 Key Research and Development Program of China (grant no. 2021YFD1500704). We
794 thank the leaders of Barangay Basper for permission to work at Basper, José June
795 Bagay and Roger Tripoli (ACIAR project) for field assistance, Cecille Marie
796 Quiñones (Visayas State University, VSU) for help with field infiltration
797 measurement, and Ofelia Maranguit and Jertz Escala (ACIAR project) for soil
798 physical analysis under supervision of Prof. Angela Ferraren (VSU). Dr. Nestor
799 Gregorio (ACIAR project), Prof. Arturo Pasa (VSU), and Prof. John Herbohn
800 (University of the Sunshine Coast) are thanked for overall facilitation of the field
801 project.

802

803 **Open Research**

804 The data used for visualization of all figures, the model input data for the 30
805 examined storm events, and the Python codes employed in the infiltration modeling
806 using GA- and SVI can be accessed via HydroShare: Cheng, Z., J. Zhang (2022).
807 Data_resource_of_figures; Model code_and_input, HydroShare,
808 <http://www.hydroshare.org/resource/6a63073f0361493f81e4e48c93fae299>

809

810 **References**

811 Allen RG, Pereira LS, Raes D, Smith M. 1998. Crop evapotranspiration – Guidelines for
812 computing crop water requirements. *FAO Irrigation and Drainage Paper 56*. UN
813 Food and Agricultural Organization, Rome.

- 814 Amoozegar A. 1989. A compact constant-head permeameter for measuring saturated
815 hydraulic conductivity of the vadose zone. *Soil Science Society of America Journal*
816 **53**: 1356–1361.
- 817 Arnold JG, Kiniry JR, Srinivasan R, Williams JR, Haney EB, Neitsch SL. 2012. *Soil and*
818 *Water Assessment Tool Input/Output Documentation Version 2012*. Texas Water
819 Resources Institute Technical Report 436. Texas A & M University, College Station,
820 TX, USA.
- 821 Aston AR, Dunin FX. 1979. Coupled infiltration and surface runoff on a 5 ha experimental
822 catchment, Karawarree, N.S.W. *Australian Journal of Soil Research* **17**: 53–64.
- 823 Bai ZG, Dent DL, Olsson L, Schaepman ME. 2008. Proxy global assessment of land
824 degradation. *Soil Use and Management* **24**: 223–234.
- 825 Beven K. 1989. Changes ideas in hydrology – The case of physically-based models. *Journal*
826 *of Hydrology* **105**: 157–172.
- 827 Birch AL, Stallard RF, Barnard HR. 2021a. Precipitation characteristics and land cover
828 control wet season runoff source and rainfall partitioning in three humid tropical
829 catchments in central Panama. *Water Resources Research* **57**, DOI:
830 10.1029/2020WR028058
- 831 Birch AL, Stallard RF, Bush SA, Barnard HR. 2021b. The influence of land cover and storm
832 magnitude on hydrologic flowpath activation and runoff generation in steep tropical
833 catchments of central Panama. *Journal of Hydrology* **596**, 126138. DOI:
834 10.1016/j.jhydrol.2021.126138
- 835 Birkel C, Correa Barahona A, Duvert C, Granados Bolaños S, Chavarría Palma A, Durán
836 Quesada, Sánchez Murillo R, Bester H. 2021. End Member and Bayesian mixing
837 models consistently indicate near-surface flowpath dominance in a pristine humid
838 tropical rainforest. *Hydrological Processes* **35 (4)**, DOI: 10.1002/hyp.14153
- 839 Blanchart E, Albrecht A, Brown G, Decaens T, Duboisset A, Lavelle P, Mariani L, Roose E.
840 2004. Effects of tropical endogeic earthworms on soil erosion. *Agriculture,*
841 *Ecosystems & Environment* **104**: 303–315.
- 842 Blöschl G, Sivapalan M. 1995. Scales issues in hydrological modelling: a review.
843 *Hydrological Processes* **9**: 251–290. DOI:10.1002/hyp.3360090305
- 844 Bonell M, Purandara BK, Venkatesh B, Krishnaswamy J, Acharya HAK, Singh UV,
845 Jayakumar R, Chappell NA. 2010. The impact of forest use and reforestation on soil
846 hydraulic conductivity in the Western Ghats of India: implications for surface and
847 sub-surface hydrology. *Journal of Hydrology* **391**: 47–62.
848 DOI:10.1016/j.jhydrol.2010.07.004
- 849 Bos MG. 1989. *Discharge measurement structures*, 3rd Ed. *ILRI Publication* 20. International
850 Institute for Land Reclamation and Improvement: Wageningen, the Netherlands, 401
851 p.
- 852 Brooks ES, Boll J, McDaniel PA. 2004. A hillslope-scale experiment to measure lateral
853 saturated hydraulic conductivity. *Water Resources Research* **40**, **W04208**. DOI:
854 10.1029/2003WR002858
- 855 Bruijnzeel LA. 1988. Estimates of evaporation in plantations of *Agathis dammara* Warb. In
856 South-Central Java, Indonesia. *Journal of Tropical Forest Science* **1**: 145–161.

- 857 Bruijnzeel LA. 2004. Hydrological functions of tropical forests: not seeing the soil for the
858 trees? *Agriculture, Ecosystems & Environment* **104**: 185–228. DOI:
859 10.1016/j.agee.2004.01.015
- 860 Brutsaert W. 2005. Infiltration and related unsaturated flows. Chapter 6 in *Hydrology: An*
861 *introduction*. Cambridge University Press, Cambridge, UK. 307–365.
- 862 Bush SA, Stallard RF, Ebel BA, Barnard HR. 2020. Assessing plot-scale impacts of land use
863 on overland flow generation in Central Panama. *Hydrological Processes* **34**: 5043–
864 5069. DOI: 10.1002/hyp.13924
- 865 Campos Pinto L, de Mello CR, Norton LD, Poggere GC, Owens PR, Curi N. 2018. A
866 hydropedological approach to a mountainous clayey Humic Dystrudept in the
867 Mantiqueira Range, southeastern Brazil. *Scientia Agricola* **75**: 60–69. DOI:
868 10.1590/1678-992X-2016-0144
- 869 Chandler DG, Walter MF. 1998. Runoff responses among common land uses in the uplands
870 of Matalom, Leyte, Philippines. *Transactions of the American Society of Agricultural*
871 *Engineers*: **41**: 1635–1641.
- 872 Chappell NA, Franks SW, Larenus J. 1998. Multi-scale permeability estimation for a tropical
873 catchment. *Hydrological Processes* **12**: 1507–1523.
- 874 Chappell NA, Bonell M, Barnes CJ, Tych W. 2012. Tropical cyclone effects on rapid runoff
875 responses: quantifying with new continuous-time transfer function models.
876 *International Association of Hydrological Sciences Publication* **353**: 82–92.
- 877 Chappell NA, McKenna P, Bidin K, Douglas I, Walsh RPD. 1999. Parsimonious modelling of
878 water and suspended-sediment flux from nested-catchments affected by selective
879 tropical forestry. *Philosophical Transactions of the Royal Society (London) Series B*
880 **354**: 1831–1846.
- 881 Chappell NA, Tych W, Chotai A, Bidin K, Sinun W, Thang HC. 2006. BARUMODEL:
882 combined Data Based Mechanistic models of runoff response in a managed rainforest
883 catchment. *Forest Ecology and Management* **224**: 58–80.
- 884 Cheng Y, Ogden FL, Zhu J., Bretfeld M. 2018. Land use-dependent preferential flow paths
885 affect hydrological response of steep tropical lowland catchments with saprolitic
886 soils. *Water Resources Research* **54**, WR021875. DOI: 10.1029/2017WR021875
- 887 Cinco TA, de Guzman RG, Ortiz AMD, Delfino RJP, Lasco RD, Hilario FD, Juanillo EL,
888 Barba R, Ares, ED. 2016. Observed trends and impacts of tropical cyclones in the
889 Philippines. *International Journal of Climatology* **36**: 4638–4650. DOI:
890 10.1002/joc.4659
- 891 Chu ST. 1978. Infiltration during an unsteady rain. *Water Resources Research* **14**: 461–466.
- 892 Concepcion RN, Samar ED. 1995. Grasslands: development attributes, limitations and
893 potentials. In *Strengthening research and development for sustainable management of*
894 *grasslands*, Bravo MVA, Exconde AB (eds). Forest Research Institute, College:
895 Laguna, The Philippines. 110–116.
- 896 Connolly RD, Silburn DM, Ciesiolka CAA. 1997. Distributed parameter hydrology model
897 (ANSWERS) applied to a range of catchment scales using rainfall simulator data. III.
898 Application to a spatially complex catchment. *Journal of Hydrology* **193**: 183–203.
- 899 Coughlan KJ. 1997. Description of sites, experimental treatments and methodology. In *A new*
900 *soil conservation methodology and application to cropping systems in tropical*

901 *steeplands*, Coughlan KJ, Rose CW (eds). ACIAR, Canberra, Australia. 3–8.

902 Davis SH, Vertessy RA, Silberstein RP. 1999. The sensitivity of a catchment model to soil

903 hydraulic properties obtained by using different measuring techniques. *Hydrological*

904 *Processes* **13**: 677–688.

905 Dickinson WT, Whiteley H. 1970. Watershed areas contributing to runoff. *International*

906 *Association of Hydrological Sciences Publication* **1**: 12–26.

907 Dubreuil P. 1985. Review of field observations of runoff generation in the tropics. *Journal of*

908 *Hydrology* **80**: 237–264.

909 Dunne T, Black RD. 1970. Partial area contributions to storm runoff in a small New England

910 watershed. *Water Resources Research* **6**: 1296–1311.

911 Dunne T, Zhang WH, Aubry BF. 1991. Effects of rainfall, vegetation, and microtopography

912 on infiltration and runoff. *Water Resources Research* **27**: 2271–2285.

913 Durán-Zuazo VH, Rodríguez-Pleguezuelo CR. 2008. Soil erosion and runoff prevention by

914 plant covers: a review. *Agronomy for sustainable Development* **28**: 65–86.

915 Fentie B, Yu B, Silburn MD, Ciesiolka CAA. 2002. Evaluation of eight different methods to

916 predict hillslope runoff rates for a grazing catchment in Australia. *Journal of*

917 *Hydrology* **261**: 102–114.

918 Flanagan DC, Ascough II, JC, Nearing MA, Laflen JM. 2001. The water erosion prediction

919 project (WEPP). In *Landscape erosion and evolution modelling*, Harmon RS, Doe III

920 WW (eds). Kluwer Academic Publishers: New York. 145–199.

921 Garen DC, Moore DS. 2005. Curve Number hydrology in water quality modeling: uses,

922 abuses, and future directions. *Journal of the American Water Resources Association*

923 **41**: 377–388.

924 Garrity DP, Soekardi M, van Noordwijk M, de la Cruz R, Pathak PS, Gunasena HPM, Van So

925 N, Huijun G, Majid NM. 1997. The *Imperata* grasslands of tropical Asia: area,

926 distribution, and typology. *Agroforestry Systems* **36**: 3–19.

927 Ghimire CP, Zwartendijk BW, Pde F, Bruijnzeel LA. 2021. Changes in soil hydraulic

928 conductivity and preferential flow pathways after assisted forest restoration on

929 degraded land in the Khasi Hills (Meghalaya, India). Abstract of oral presentation at

930 the EGU General Assembly 2021, EGU 21-6559.

931 Ghimire CP, Bonell M, Bruijnzeel LA, Coles NA, Lubczynski MW. 2013. Reforesting

932 severely degraded grassland in the Lesser Himalaya of Nepal: effects on soil

933 hydraulic conductivity and overland flow production, *Journal of Geophysical*

934 *Research: Earth Surface* **118**: 2528–2545. DOI: 10.1002/2013JF002888.

935 Gibbs HKG, Salmon JM. 2015. Mapping the world’s degraded lands. *Applied Geography* **57**:

936 12–21.

937 Gupta HV, Sorooshian S, Yapo PO. 1999. Status of automatic calibration for hydrologic

938 models: Comparison with multilevel expert calibration. *Journal of Hydrologic*

939 *Engineering* **4(2)**: 135–143.

940 Hawkins RH. 1982. Interpretations of source area variability in rainfall-runoff relations. In

941 *Rainfall-runoff relationships*, VP Singh (ed.), Water Resources Publications: Littleton

942 CO, USA. 302–324.

943 Hawkins RH, Cundy TW. 1987. Steady-state analysis of infiltration and overland flow for

944 spatially-varied hillslopes. *Water Resources Bulletin* **23**: 251–256.

- 945 Hewlett JD, Hibbert AR. 1967. Factors affecting the response of small watersheds to
 946 precipitation in humid areas. In *International symposium on forest hydrology*, WE
 947 Sopper, HW Lull (eds). Pergamon Press: Oxford, UK. 275–290.
- 948 James WP, Warinner J, Reedy M. 1992. Application of the Green-Ampt infiltration equation
 949 to watershed modeling. *Water Resources Bulletin* **28**: 623–635.
- 950 Jasmin BB. 1976. Grassland uses: effect on surface runoff and sediment yield. *SYLVATROP*
 951 *Philippines Forest Research Journal* **1**: 156–172.
- 952 Koorevaar P, Menelik G, Dirksen C. 1983. *Elements of soil physics. Developments in Soil*
 953 *Science* **13**. Elsevier Science Ltd: Amsterdam, The Netherlands, 229 p.
- 954 Lacombe G, Valentin C, Sounyagong P, de Rouw A, Souleuth B, Silvera N, Pierret A,
 955 Sengthaheuanghoung O, Ribolzi O. 2018. Linking crop structure, throughfall, soil
 956 surface conditions, runoff and soil detachment: 10 land uses analyzed in Northern
 957 Laos. *Science of the Total Environment* **616–617**: 1330–1338.
 958 <https://doi.org/10.1016/j.scitotenv.2017.10.185>
- 959 Lai JB, Ren L. 2007. Assessing the size dependency of measured hydraulic conductivity using
 960 double-ring infiltrometers and numerical simulation. *Soil Science Society of America*
 961 *Journal* **71**: 1667–1675. DOI: 10.2136/sssaj2006.0227
- 962 Lapides DA, Hahm WJ, Rempe DM, Dietrich WE, Dralle DN. 2022. Controls on streamwater
 963 age in a saturation overland flow-dominated catchment. *Water Resources Research*
 964 **58**, WR031665. DOI: 10.1029/2021WR031665
- 965 Leemhuis C, Erasmi S, Twele A, Kreilein H, Oltchev A, Gerold G. 2007. Rainforest
 966 conversion in central Sulawesi, Indonesia: recent development and consequences.
 967 *Erdkunde* **61**: 284–293.
- 968 Legates DR, McCabe GJ. 1999. Evaluating the use of ‘goodness-of-fit’ measures in
 969 hydrologic and hydroclimatic model validation. *Water Resources Research* **35**: 233–
 970 241.
- 971 Leopoldo PR, de Pádua Sousa A, Filho ST. 1981. Rainfall interception by a sugarcane crop.
 972 *Brasil Açcaiceiro* **6**: 9–16 (in Portuguese, with abstract in English).
- 973 Limsuan MP. 1995. Impacts of grassland use manipulation on water quantity and quality in
 974 Angat, Bulacan, Philippines. In *Strengthening research and development for*
 975 *sustainable management of grasslands*, Bravo MVA, Exconde AB (eds). Forest
 976 Research Institute: College, Laguna, The Philippines. 136–142.
- 977 Liu WJ, Liu W, Lu H, Duan W, Li HM. 2011. Runoff generation in small catchments under a
 978 native rainforest and a rubber plantation in Xishuangbanna, southwest China. *Water*
 979 *and Environment Journal* **25**: 138–147. DOI: 10.1111/j.1747-6593.2009.0211.x
- 980 Marquardt DW. 1963. An algorithm for least-squares estimation of nonlinear parameters.
 981 *Journal of the Society for Industrial and Applied Mathematics* **11**: 431–441.
- 982 Martinez LJ, Zinck JA. 2004. Temporal variation of soil compaction and deterioration of soil
 983 quality in pasture areas of Colombian Amazonia. *Soil and Tillage Research* **75**: 3–17.
 984 DOI: 10.1016/j.still.2002.12.001
- 985 Mathys N, Meunier M, Brochot S. 1996. The forest effect on floods in small mountainous
 986 catchments: some results from experimental catchments of Draix, France. In
 987 *Conference on Ecohydrological Processes in Small Basins*, Strasbourg, France, 24 –
 988 26 September 1996. 123–128.

- 989 Mein RG, Larsen CL. 1973. Modeling infiltration during a steady rain. *Water Resources*
990 *Research* **9**: 384–394.
- 991 Mertens J, Madsen H, Kristensen M, Jacques D, Feyen J. 2005. Sensitivity of soil parameters
992 in unsaturated zone modelling and the relation between effective, laboratory and *in*
993 *situ* estimates. *Hydrological Processes* **19**: 1611–1633. DOI: 10.1002/hyp.5591
- 994 Miyata S, Kosugi K, Gomi T, Mizuyama T. 2009. Effects of forest floor coverage on overland
995 flow and soil erosion on hillslopes in Japanese cypress plantation forests. *Water*
996 *Resources Research* **45**, W06402. <https://doi.org/10.1029/2008WR007270>
- 997 Molina A, Govers G, Vanacker V, Poesen J, Zeelmaekers E, Cisneros F. 2007. Runoff
998 generation in a degraded Andean ecosystem: interaction of vegetation and land use.
999 *Catena* **71**: 357–370. DOI: 10.1016/j.catena.2007.04.002
- 1000 Nash JE, Sutcliffe JV. 1970. River flow forecasting through conceptual models. Part I – A
1001 discussion of principles. *Journal of Hydrology* **10**: 282–290. DOI: 10.1016/0022-
1002 1694(70)90255-6
- 1003 Nearing MD, Liu BY, Risse LM, Zhang X. 1996. Curve numbers and Green-Ampt effective
1004 hydraulic conductivities. *Water Resources Bulletin* **32**: 125–136.
- 1005 Neitsch SL, Arnold JG, Kiniry JR, Willams JR. 2011. Soil Water Assessment Tool –
1006 Theoretical Documentation. Texas Water Resources Institute Technical Report 406.
1007 Texas A & M University, College Station, TX, USA.
- 1008 Obiero JPO. 1996. *Evaluation of infiltration using the Green-Ampt model and rainfall-runoff*
1009 *data for Lagan and Sambret catchments, Kericho, Kenya*. MSc Thesis, University of
1010 Nairobi, Nairobi, Kenya, 124 pp.
- 1011 Ogden FL, Hawkins RP, Walter MT, Goodrich DC. 2017. Comment on “Beyond the SCS-CN
1012 method: A theoretical framework for spatially-lumped rainfall-runoff response” by
1013 M. S. Bartlett et al. *Water Resources Research*. DOI: 10.1002/2016WR020176
- 1014 Quiñones CM. 2014. *Properties of soils from ultramafic rocks in the degraded grassland*
1015 *watershed in Basper, Leyte*. MSc Thesis, Visayas State University, Baybay, Leyte
1016 Island, the Philippines, 105 p.
- 1017 Patin J, Mouche E, Ribolzi O, Chaplot V, Sengtahevong O, Latsachak KO, Souleuth
1018 B, Valentin C. 2012. Analysis of runoff production at the plot scale during a long-
1019 term survey of a small agricultural catchment in Lao PDR. *Journal of Hydrology*
1020 **426–427**: 79–92. DOI: 10.1016/j.jhydrol.2012.01.015
- 1021 Pirastru M, Bagarello V, Iovino M, Marrosu R, Castellini M, Giadrossich F, Niedda M. 2017.
1022 Subsurface flow and large-scale lateral saturated soil hydraulic conductivity in a
1023 Mediterranean hillslope with contrasting land uses. *Journal of Hydrology and*
1024 *Hydromechanics* **65**: 297–306. DOI: 10.1515/johh-2017-0006
- 1025 Ponce VM, Hawkins RH. 1996. Runoff curve number: has it reached maturity? *Journal of*
1026 *Hydrologic Engineering* **1**: 11–19.
- 1027 Recha JW, Lehmann J, Walter MT, Pell A, Verchot L, Johnson M. 2012. Stream discharge in
1028 tropical headwater catchments as a result of forest clearing and soil degradation.
1029 *Earth Interactions* **16**–013, DOI:10.1175/2012EI000439.1
- 1030 Ribolzi O, Evrard, O, Huon S, de Rouw A, Silvera N, Latsachak KO, Souleuth B, Lefevre I,
1031 Pierret A, Lacombe G, Sengtahevong O, Valentin C. 2017. From shifting
1032 cultivation to teak plantation: effects on overland flow and sediment yield in a

- 1033 montane tropical catchment. *Scientific Reports* **7**:3987. DOI: 10.1038/s41598-017-
1034 04385-2
- 1035 Ribolzi O, Lacombe G, Pierret A, Robain H, Sounyafong P, de Rouw A, Soullieuth B,
1036 Mouche E, Huon S, Silvera N, Latsachak KO, Sengtaheuanghoung O, Valentin C.
1037 2018. Interacting land use and soil surface dynamics control groundwater outflow in a
1038 montane catchment of the lower Mekong. *Agriculture, Ecosystems & Environment*
1039 **268**: 90–102. DOI: 10.1016/j.agee.2018.09.005
- 1040 Rose CW, Coughlan KJ, Ciesiolka CAA, Fentie B. 1997. The role of soil cover in soil
1041 conservation. In *A new soil conservation methodology and application to cropping*
1042 *systems in tropical steeplands*, Coughlan KJ, Rose CW (eds). ACIAR, Canberra,
1043 Australia. 59–78.
- 1044 Shaw EM, Beven KJ, Chappell NA, Lamb R. 2010. *Hydrology in practice*, 4th Ed. CRC Press:
1045 Boca Raton FL, USA.
- 1046 Sharma ML, Barron RJW, Fernie MS. 1987. Areal distribution of infiltration parameters and
1047 some soil physical properties in lateritic catchments. *Journal of Hydrology* **94**: 109–
1048 127.
- 1049 Sherlock MD, Chappell NA, McDonnell JJ. 2000. Effects of experimental uncertainty on the
1050 calculation of hillslope flow paths. *Hydrological Processes* **14**: 2457–2471.
- 1051 Shougrakpam S, Sarkar R, Dutta S. 2010. An experimental investigation to characterise soil
1052 macroporosity under different land use and land covers of northeast India. *Journal of*
1053 *Earth System Science* **119**: 655–674.
- 1054 Sidle RC Ziegler AD, Negishi JN, Rahim Nik A, Siew R, Turkelboom F. 2006. Erosion
1055 processes in steep terrain – Truths, myths, and uncertainties related to forest
1056 management in Southeast Asia. *Forest Ecology & Management* **224**: 199–225. DOI:
1057 10.1016/j.foreco.2005.12.019
- 1058 Sirimarco X, Barral MP, Villarino SH, Laterra P. 2018. Water regulation by grasslands: a
1059 global meta-analysis. *Ecohydrology*, <https://doi.org/10.1002/eco.1934>
- 1060 Stone JJ, Paige GB, Hawkins RH. 2008. Rainfall intensity-dependent infiltration rates on
1061 rangeland rain-fall simulator plots. *Transactions of the American Society of*
1062 *Agricultural Engineers* **51**: 45–53.
- 1063 Sutherland RA, Bryan RB. 1990. Runoff and erosion from a small semiarid catchment,
1064 Baringo District, Kenya. *Applied Geography* **10**: 91–109.
- 1065 Taylor CJ, Pedregal DJ, Young PC, Tych W. 2007. Environmental time series analysis and
1066 forecasting with the CAPTAIN toolbox. *Environmental Modeling & Software* **22**:
1067 797–814.
- 1068 Toohey RC, Boll J, Brooks ES, Jones JR. 2018. Effects of land use on soil properties and
1069 hydrological processes at the point, plot and catchment scale on volcanic soils near
1070 Turrialba, Costa Rica. *Geoderma* **315**: 138–148. DOI:
1071 10.1016/j.geoderma.2017.11.044
- 1072 USBR. 1997. Water measurement manual, 3rd Ed. US Department of the Interior, bureau of
1073 Reclamation, Washington DC.
1074 http://www.usbr.gov/tsc/techreferences/mands/wmm/chap07_13.html
- 1075 Valentin C, Agus F, Alamban R, Boosaner A, Bricquet JP and 14 others. 2008. Runoff and
1076 sediment losses from 27 upland catchments in Southeast Asia: impacts of rapid land

- 1077 use changes and conservation practices. *Agriculture, Ecosystems & Environment* **128**:
1078 225–238. DOI: 10.1016/j.agee.2008.06.004
- 1079 Van Dijk AIJM, Bruijnzeel LA. 2004. Runoff and soil loss from bench terraces. 1. An event-
1080 based model of rainfall infiltration and surface runoff. *European Journal of Soil*
1081 *Science* **55**: 299–316. DOI: 10.1111/j.1365-2389.2004.00604.x
- 1082 Van Meerveld HJ, Zhang J, Tripoli R, Bruijnzeel LA. 2019. Effect of reforestation of a
1083 degraded *Imperata* grassland on dominant flow pathways and streamflow responses
1084 in Leyte, the Philippines. *Water Resources Research* **55**, DOI:
1085 10.1029/2018WR023896
- 1086 Van Mullem JA. 1991. Runoff and peak discharges using Green-Ampt infiltration model.
1087 *Journal of Hydrologic Engineering* **117**: 354–370.
- 1088 Waterloo MJ, Bruijnzeel LA, Vugts HJ, Rawaq TT. 1999. Evaporation from Pinus caribaea
1089 plantations on former grassland soils under maritime tropical conditions. *Water*
1090 *Resources Research* **35**: 2133–2144.
- 1091 Wen X, Gomez-Hernandez JJ. 1996. Upscaling hydraulic conductivities in heterogeneous
1092 media: A review. *Journal of Hydrology* **183**: 9-32.
- 1093 White JT, Hunt RJ, Fienen MN, Doherty JE. 2020. Approaches to highly parameterized
1094 inversion: PEST++ Version 5, a Software suite for parameter estimation, uncertainty
1095 analysis, management optimization and sensitivity analysis. *US Geological Survey*
1096 *Techniques and Methods* **7C26**, 52 p.
1097 <https://pubs.er.usgs.gov/publication/tm7C26>
- 1098 Wiersum KF. 1985. Effects of various vegetation layers in an *Acacia auriculiformis* forest
1099 plantation on surface erosion in Java, Indonesia. In: *Soil Erosion and Conservation*,
1100 El-Swaify S, Moldenhauer WC, Lo A. (Eds.). Soil Conservation Society of America:
1101 Ankeny, Wisconsin, pp. 79–89.
- 1102 Yamamoto, EMS, Sayama T, Yamamoto K, Apip A. 2020. Comparison of runoff generation
1103 methods for land use impact assessment using the SWAT model in humid tropics.
1104 *Hydrological Research Letters* **14**: 81–88. DOI: 10.3178/hrll.14.81
- 1105 Yin J, Gentine P, Zhou S, Sullivan SC, Wang R, Zhang Y, Guo SL. 2019. Large increase in
1106 global runoff extremes driven by climate and anthropogenic changes. *Nature*
1107 *Communications* (2018) **9**:4389. DOI: 10.1038/s41467-018-06765-2
- 1108 Yira Y, Diekkrüger B, Steup G, Bossa AY. 2016. Modeling land use change impacts on water
1109 resources in a tropical West African catchment (Dano, Burkina Faso). *Journal of*
1110 *Hydrology* **537**: 187–199. DOI: 10.1016/j.jhydrol.2016.03.052
- 1111 Young PC. 2001. Data-Based Mechanistic modelling and validation of rainfall–flow
1112 processes. In *Model validation: perspectives in hydrological science*, Anderson MG,
1113 Bates PG (eds). Wiley & Sons: Chichester, UK. 117–161.
- 1114 Yu B. 1999. A comparison of the Green–Ampt and a spatially variable infiltration model for
1115 natural storm events. *Transactions of the American Society of Agricultural*
1116 *Engineering* **42**: 89–97.
- 1117 Yu B. 2005. Process-based erosion modelling: promises and progress. In *Forests, water and*
1118 *people in the humid tropics*, Bonell M, Bruijnzeel LA (eds). Cambridge University
1119 Press: Cambridge, UK. 790–810.

- 1120 Yu B. 2012. Validation of SCS method for runoff estimation. *Journal of Hydrologic*
 1121 *Engineering* **2012.17**: 1158–1163.
- 1122 Yu B, Rose CW, Coughlan FJ, Fentie B. 1997a. Plot-scale rainfall-runoff characteristics and
 1123 modelling at six sites in Australia and South East Asia. *Transactions of the American*
 1124 *Society of Agricultural Engineering* **40**: 1295–1303.
- 1125 Yu B, Rose CW, Coughlan KJ, Fentie B. 1997b. Plot-scale runoff modelling for soil loss
 1126 prediction. In *A new soil conservation methodology and application to cropping*
 1127 *systems in tropical steplands*, Coughlan KJ, Rose CW (eds). ACIAR, Canberra,
 1128 Australia. 24–33.
- 1129 Yu B, Rose CW, Ciesiolka CCA, Cakurs U. 2000. The relationship between runoff rate and
 1130 lag time and the effects of surface treatments at the plot scale. *Hydrological Sciences*
 1131 *Journal* **45**: 709–726.
- 1132 Yu B, Sombatanit S, Rose CW, Ciesiolka CAA, Coughlan KJ. 2000. Characteristics and
 1133 modeling of runoff hydrographs for different tillage treatments. *Soil Science Society*
 1134 *of America Journal* **64**: 1763–1770.
- 1135 Zehe E, Flüßler W. 2001. Slope-scale variation of flow patterns in soil profiles. *Journal of*
 1136 *Hydrology* **247**: 116–132. DOI: 10.1016/S0022-1694(01)00371-7
- 1137 Zhang J, van Meerveld HJ, Tripoli, R, Bruijnzeel LA. 2018a. Runoff response and sediment
 1138 yield of a landslide-affected fire-climax grassland catchment (Leyte, The Philippines)
 1139 before and after passage of typhoon Haiyan. *Journal of Hydrology* **565**: 524–537.
 1140 DOI: 10.1016/j.jhydrol.2018.08.016
- 1141 Zhang J, Bruijnzeel LA, Tripoli R, van Meerveld HJ. 2018b. Water budget and run-off
 1142 response of a tropical multispecies “reforest” and effects of typhoon disturbance.
 1143 *Ecohydrology* 2018; e2055. <https://doi.org/10.1002/eco.2055>
- 1144 Zhang J, Bruijnzeel LA, Quiñones MC, Tripoli R, Asio VB, van Meerveld HJ. 2019a.
 1145 Comparative soil physical characteristics of a fire-climax grassland and a multi-
 1146 species reforest (Leyte, the Philippines): implications for runoff generation.
 1147 *Geoderma* **333**: 163–177. DOI: 10.1016/j.geoderma.2018.07.022
- 1148 Zhang J, Tych W, Chappell N, van Meerveld HJ, Bruijnzeel LA. 2019b. Separating effects of
 1149 rainfall variability and typhoon disturbance on the runoff response of a tropical
 1150 ‘reforest’ using a data-based mechanistic modeling approach. Abstract EGU2019-
 1151 10222. Annual Assembly of the European Geophysical Union, Vienna, April 2019.
- 1152 Ziegler AD, Giambelluca TW, Tran LT, Vana TT, Nullet MA, Fox J, Vien TD, Pinthong J,
 1153 Maxwell JF, Evett S. 2004. Hydrological consequences of landscape fragmentation in
 1154 mountainous northern Vietnam: evidence of accelerated overland flow generation.
 1155 *Journal of Hydrology* **287**: 124–146. DOI: 10.1016/j.jhydrol.2003.09.027
- 1156 Ziegler AD, Bruun TB, Guardiola-Claramonte M, Giambelluca TW, Lawrence D, Thanh
 1157 Lam N. 2009. Environmental consequences of the demise in swidden cultivation in
 1158 montane mainland Southeast Asia: hydrology and geomorphology. *Human Ecology*
 1159 **37**: 361–373. DOI: 10.1007/s10745-009-9258-x
- 1160 Zimmermann B, Elsenbeer H, De Moraes JM. 2006. The influence of land-use changes on
 1161 soil hydraulic properties: implications for runoff generation. *Forest Ecology and*
 1162 *Management* **222**: 29–38. DOI: 10.1016/j.foreco.2005.10.070
- 1163 Zwartendijk BW, van Meerveld HJ, Ghimire CP, Bruijnzeel LA, Ravelona M, Jones JPG.

1164 2017. Rebuilding soil hydrological functioning after swidden agriculture in eastern
1165 Madagascar. *Agriculture, Ecosystems & Environment* **239**: 101–111. DOI:
1166 10.1016/j.agee.2017.01.002

1167
1168

1169 **References From the Supporting Information**

1170 Bonell M, Barnes CJ, Grant CR, Howard A, Burns J. 1998. High rainfall, response-dominated
1171 catchments: a comparative study of experiments in tropical northeast Queensland
1172 with temperate New Zealand. In: *Isotope tracers in catchment hydrology*, Kendall C,
1173 McDonnell JJ (Eds.). Elsevier, Amsterdam, 347–390.

1174 *Chappell NA, Bonell M, Barnes CJ, Tych W. 2012. Tropical cyclone effects on rapid runoff
1175 responses: quantifying with new continuous-time transfer function models.
1176 *International Association of Hydrological Sciences Publication* **353**: 82–92.

1177 *Chappell NA, McKenna P, Bidin K, Douglas I, Walsh RPD. 1999. Parsimonious modelling
1178 of water and suspended-sediment flux from nested-catchments affected by selective
1179 tropical forestry. *Philosophical Transactions of the Royal Society (London) Series B*
1180 **354**: 1831–1846.

1181 *Coughlan KJ. 1997. Description of sites, experimental treatments and methodology. In *A*
1182 *new soil conservation methodology and application to cropping systems in tropical*
1183 *steeplands*, Coughlan KJ, Rose CW (eds). ACIAR, Canberra, Australia. 3–8.

1184

1185 *Van Dijk AIJM, Bruijnzeel LA. 2004. Runoff and soil loss from bench terraces. 1. An event-
1186 based model of rainfall infiltration and surface runoff. *European Journal of Soil*
1187 *Science* **55**: 299–316. DOI: 10.1111/j.1365-2389.2004.00604.x

1188 *Yu B, Rose CW, Coughlan KJ, Fentie B. 1997b. Plot-scale runoff modelling for soil loss
1189 prediction. In *A new soil conservation methodology and application to cropping*
1190 *systems in tropical steeplands*, Coughlan KJ, Rose CW (eds). ACIAR, Canberra,
1191 Australia. 24–33.

1192

1193 *Note: *references from the supporting information have been listed in the main reference list.*